MASTERARBEIT | MASTER'S THESIS

Titel | Title

Screening of Natural Products and Derivatives as Modulators of ROR β

verfasst von | submitted by

Magdalena Sofie Holzer BSc

angestrebter akademischer Grad | in partial fulfilment of the requirements for the degree of

Magistra pharmaciae (Mag. pharm.)

Wien | Vienna, 2026

Studienkennzahl lt. Studienblatt | Degree programme code as it appears on the student record sheet:	UA 066 605
Studienrichtung lt. Studienblatt | Degree programme as it appears on the student record sheet:	Masterstudium Pharmazie
Betreut von | Supervisor:	Univ.-Prof. Dr. Verena Dirsch
Mitbetreut von | Co-Supervisor:	Mag. Dr. Patrik Schwarz

Table of content

Abstract

Retinoic acid receptor-related orphan receptor beta (RORβ) is a nuclear receptor that remains largely understudied compared with RORα and RORγ. Although RORβ has long been associated mainly with neuronal and retinal functions, recent findings point to an emerging role in bone biology, opening new questions about its broader biological relevance. Therefore, the identification of compounds affecting RORβ-mediated transactivation activity may provide valuable starting points to explore the function of this receptor and its potential relevance as a future therapeutic target.

In this study, selected natural products and derivatives were screened for their potential activity on RORβ using luciferase reporter gene assays in HEK293 cells. A Gal4-RORβ luciferase assay was made functional by implementing SR20156 as a reference inverse agonist. Active compounds were further tested in full-length RORβ, as well as Gal4-RORα, Gal4-RORγ, and full-length RORγ reporter assays to assess receptor subtype-dependent effects. Resazurin conversion assays were performed to evaluate effects on cell metabolic activity.

SR20156 confirmed the responsiveness of the Gal4-RORβ assay. Among the compounds selected for follow-up analysis, epicorosolic acid (SD5), its C2 epimer corosolic acid (SD2), and the phytoecdysteroid derivative CR27 were investigated in more detail. SD5 reduced RORβ-mediated transactivation activity in both the Gal4-RORβ and full-length RORβ assays, whereas the structurally related compound SD2 showed no relevant activity on RORβ under the tested conditions. In contrast, both SD5 and SD2 reduced RORγ-dependent transactivation activity. CR27 increased transactivation activity in RORβ assays. Resazurin conversion assays showed no relevant reduction in cell metabolic activity for SD5, SD2, or CR27 at the tested concentrations. However, reporter control assays indicated that the CR27-induced increase in transactivation activity may partly result from reporter-associated activity.

In conclusion, this thesis identified SD5 and CR27 as compounds affecting RORβ reporter assay activity. By comparing SD5 with its C2 epimer SD2, this work further highlights how subtle structural differences may shape receptor subtype-dependent activity within the ROR family. These findings provide a basis for further studies on potential RORβ

modulators and may support future investigations into the selectivity and biological relevance of RORβ-targeting compounds.

Zusammenfassung

Der Retinsäure-Rezeptor-verwandte Orphan-Rezeptor Beta (RORβ) ist ein nukleärer Rezeptor, der im Vergleich zu RORα und RORγ bislang weitgehend wenig untersucht ist. RORβ wird vor allem mit neuronalen und retinalen Funktionen Verbindung gebracht. Neuere Erkenntnisse deuten jedoch darauf hin, dass RORβ auch in der Knochenbiologie eine bedeutende Rolle spielen könnte. Die Identifizierung von Verbindungen, die die RORβ-vermittelte Transaktivierungsaktivität beeinflussen, könnte daher die weitere Erforschung der biologischen Funktion und potenziellen therapeutischen Relevanz dieses Rezeptors unterstützen.

In dieser Arbeit wurden ausgewählte Naturstoffe und Derivate mithilfe von Luciferase-Reporter-Gen-Assays in HEK293-Zellen auf ihre potenzielle Aktivität an RORβ untersucht. Die Implementierung von SR20156 als Referenz-Inversagonist ermöglichte die Funktionalität des Gal4-RORβ-Luciferase-Assays. Aktive Verbindungen wurden anschließend in einem *Full-length*-RORβ-Assay sowie in weiteren ROR-Reporter-Assays getestet, um rezeptorsubtypabhängige Effekte zu beurteilen. Zusätzlich wurden Resazurin-Conversion-Assays durchgeführt, um Effekte auf die metabolische Zellaktivität zu untersuchen.

SR20156 bestätigte die Responsivität des Gal4-RORβ-Assays. Unter den für die weiterführende Analyse ausgewählten Verbindungen wurden Epicorosolsäure (SD5), ihr C2-Epimer Corosolsäure (SD2) sowie das Phytoecdysteroid-Derivat CR27 genauer untersucht. SD5 reduzierte die RORβ-vermittelte Transaktivierungsaktivität sowohl im Gal4-RORβ- als auch im *Full-length*-RORβ-Assay, während die strukturell verwandte Verbindung SD2 unter den getesteten Bedingungen keine relevante Aktivität an RORβ zeigte. Im Gegensatz dazu reduzierten sowohl SD5 als auch SD2 die RORγ-abhängige Transaktivierungsaktivität. CR27 erhöhte die Transaktivierungsaktivität in RORβ-Assays; Reporter-Kontrollassays deuteten jedoch darauf hin, dass dieser Effekt teilweise auf reporterassoziierte Aktivität zurückzuführen sein könnte. Resazurin-Conversion-Assays zeigten bei den getesteten Konzentrationen keine relevante Verringerung der metabolischen Zellaktivität durch SD5, SD2 oder CR27. Reporter-Kontrollassays deuteten jedoch darauf hin, dass die CR27-induzierte Erhöhung der

Transaktivierungsaktivität teilweise auf reporterassoziierte Aktivität zurückzuführen sein könnte.

Zusammenfassend lässt sich sagen, dass in dieser Arbeit SD5 und CR27 als Verbindungen identifiziert wurden, die die Aktivität des RORβ-Reporter-Assays beeinflussen. Der Vergleich von SD5 mit seinem C2-Epimer SD2 unterstreicht außerdem, dass bereits kleine strukturelle Unterschiede die rezeptorsubtypabhängige Aktivität innerhalb der ROR-Familie beeinflussen können. Diese Ergebnisse bilden eine Grundlage für weitere Untersuchungen zu potenziellen RORβ-Modulatoren und können zukünftige Studien zur Selektivität und biologischen Relevanz RORβ-gerichteter Verbindungen unterstützen.

1 Introduction

Gene expression is tightly regulated and essential for many physiological and pathological processes. Nuclear receptors are key regulators in this system, forming a superfamily of ligand-activated transcription factors that control diverse cellular functions [1,2]. Through this central role in gene regulation, nuclear receptors have become a major focus in drug discovery [1,3]. Within this superfamily, retinoic acid receptor-related orphan receptors (RORs) have gained increasing attention due to their involvement in immune regulation, metabolic control, and tissue-specific gene expression [4–6]. However RORβ remains heavily understudied, although it has been implicated in neuronal and retinal development and also has been shown to regulate gene expression in osteoblasts, suggesting a potential role in bone biology [7,8].

1.1 Nuclear receptors

When nuclear receptor signaling is disturbed, it can contribute to different pathological processes, especially in metabolic, inflammatory and cancer-related diseases [1,2]. Therefore, nuclear receptors are also relevant targets in drug discovery [1]. While endogenous ligands have been identified for many nuclear receptors, others are still classified as orphan receptors because their physiological ligands remain unknown or have not yet been clearly confirmed.

The nuclear receptor superfamily consists of ligand-dependent transcription factors that are involved in numerous biological processes, including metabolism, inflammation, reproduction, homeostasis, and circadian rhythm [1,2]. In humans, 48 nuclear receptors have been identified, most of which are regulated by the binding of small lipophilic ligands such as steroids, retinoids, and lipids. Based on sequence similarity, these receptors are classified into seven subfamilies [9]. To better understand the diverse functions and regulatory mechanisms of these receptors, recent advances in structural biology and genome-wide approaches have contributed to a deeper understanding of their function [2].

1.1.1 Structural and Functional Classification of Nuclear Receptors

Nuclear receptors can be classified based on both sequence similarity and functional properties. In this section, the functional classification is described first, as it explains key

differences in subcellular localization, dimerization behavior, ligand response, and DNA-binding mode. According to this functional classification, nuclear receptors can be grouped into type I, II, III, and IV receptors [10].

Type I nuclear receptors, also known as steroid hormone receptors, are located in the cytoplasm in their inactive state, where they are associated with heat-shock proteins (HSPs) [3,10].Upon ligand binding, they become activated, translocate into the nucleus, and bind as homodimers to specific DNA response elements, typically consisting of palindromic sequences. In contrast, type II, III, and IV nuclear receptors are primarily located in the nucleus, even in the absence of a ligand [2,10]. They are usually already bound to DNA and regulate gene expression through the exchange of co-repressors and co-activators upon ligand binding. Type II receptors form heterodimers with the retinoid X receptor (RXR) and bind to direct repeat elements, whereas type III receptors act as homodimers. Type IV receptors bind as monomers to extended half-site DNA sequences [10]. These main functional differences between type I–IV nuclear receptors, including dimerization behavior, ligand response, and DNA-binding mode, are summarized in Figure 1. Although endogenous ligands are known for some type III and IV receptors, many members remain classified as orphan receptors because their physiological ligands have not yet been clearly identified [3,10].

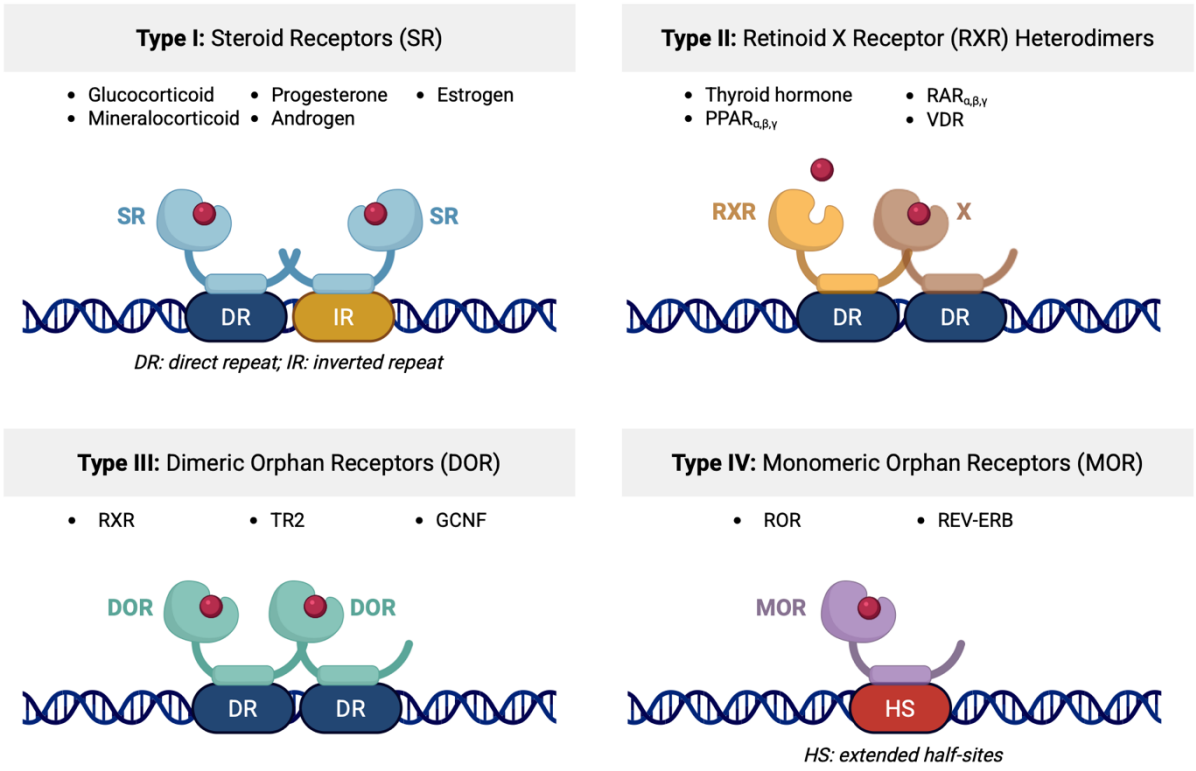

Figure 1. **Nuclear receptors type I-IV.** Overview of the four classes of nuclear receptors and their differences in dimerization, ligand response, and DNA interaction. Type I: Steroid Receptors (SR), Type II: RXR Heterodimers, Type III: Dimeric Orphan Receptors (DOR), Type IV: Monomeric Orphan Receptors (MOR). PPAR = Peroxisome proliferator-activated receptor, RAR= Retinoic acid receptor, VDR= Vitamin D receptor, RXR= Retinoid X receptor, TR2=Testicular receptor 2, GCNF = Germ cell nuclear factor, ROR = Retinoic acid-related orphan receptor. Adapted from [3,11], created with BioRender.com

1.1.2 Structural organization of nuclear receptors

Nuclear receptors share a conserved modular architecture composed of several functional domains (A–E), as illustrated in Figure 2. These include two well-defined regions: a central DNA-binding domain (DBD) and a C-terminal ligand-binding domain (LBD). The N-terminal region (A/B domain) is highly variable in size and sequence and contains the ligand-independent activation function-1 (AF-1), which mediates transcriptional activation through interactions with co-regulator proteins. The DNA-binding domain (DBD, C domain) is the most structurally conserved region among nuclear receptors and consists of two zinc finger motifs that enable sequence-specific binding to DNA response elements and contribute to receptor dimerization [2,11]. In some receptors, C-terminal extensions (CTEs) provide additional contacts with the DNA [11]. A

flexible hinge region (D domain) connects the DBD and LBD and contains nuclear localization signals. The ligand-binding domain (LBD, E domain), located within the C-terminal region, forms a hydrophobic pocket that binds lipophilic ligands. Ligand binding induces conformational changes, particularly of helix 12, which regulates the ligand-dependent activation function-2 (AF-2) and the recruitment of co-activators or co-repressors [2,11].

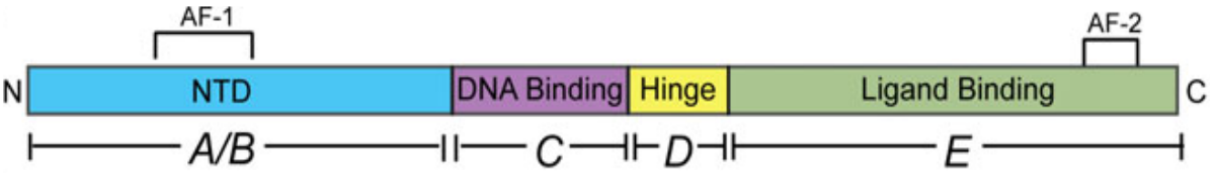

Figure 2. **Modular domain architecture of nuclear receptors.** Nuclear receptors consist of an N-terminal A/B domain containing AF-1, a DNA-binding domain (C), a hinge region (D), and a C-terminal ligand-binding domain (E) containing AF-2. [2]

Taken together, nuclear receptors share a conserved domain organization but differ in their sequence, ligand specificity, dimerization behavior, and DNA-binding mode [2,10]. In addition to the functional classification described above, the official nomenclature classifies human nuclear receptors according to sequence similarity into seven subfamilies, designated NR0 to NR6 [12]. Table 1 provides an overview of selected human nuclear receptors, including their subfamily, abbreviation, and reported ligands.

Table 1. **Overview of the nuclear receptor superfamily[2]**

Subfamily	Name	Abbreviation	Ligand
0B	Dosage-sensitive sex reversal-adrenal hypoplasia congenital critical region on the X chromosome, Gene 1	DAX1	Orphan
	Short heterodimeric partner	SHP	Orphan
1A	Thyroid hormone receptor-α	TRα	Thyroid hormones
	Thyroid hormone receptor-β	TRβ	Thyroid hormones
1B	Retinoic acid receptor-α	RARα	Retinoic acids
	Retinoic acid receptor-β	RARβ	Retinoic acids
	Retinoic acid receptor-γ	RARγ	Retinoic acids
1C	Peroxisome proliferator-activated receptor-α	PPARα	Fatty acids
	Peroxisome proliferator-activated receptor-β	PPARβ	Fatty acids

Subfamily	Name	Abbreviation	Ligand
	Peroxisome proliferator-activated receptor-γ	PPARγ	Fatty acids
1D	Reverse-Erb-α	REV-ERBα	Heme
	Reverse-Erb-β	REV-ERBβ	Heme
1F	Retinoic acid-related orphan receptor-α	RORα	Sterols
	Retinoic acid-related orphan receptor-β	RORβ	Sterols
	Retinoic acid-related orphan receptor-γ	RORγ	Sterols
1H	Farnesoid X receptor-α	FXRα	Bile acids
	Farnesoid X receptor-β	FXRβ	Orphan
	Liver X receptor-α	LXRα	Oxysterols
	Liver X receptor-β	LXRβ	Oxysterols
1I	Vitamin D receptor	VDR	1α, 25-dihydroxyvitamin D3
	Pregnane X receptor	PXR	Endobiotics and xenobiotics
	Constitutive androstane receptor	CAR	Xenobiotics
2A	Hepatocyte nuclear Factor-4-α	HNF4α	Fatty acids
	Hepatocyte nuclear Factor-4-γ	HNF4γ	Fatty acids
2B	Retinoid X receptor-α	RXRα	9-cis retinoic acid
	Retinoid X receptor-β	RXRβ	9-cis retinoic acid
	Retinoid X receptor-γ	RXRγ	9-cis retinoic acid
2C	Testicular receptor 2	TR2	Orphan
	Testicular receptor 4	TR4	Orphan
2E	Tailless homolog orphan receptor	TLX	Orphan
	Photoreceptor-cell-specific nuclear receptor	PNR	Orphan
2F	Chicken ovalbumin upstream promotor-transcription factor α	COUP-TFα	Orphan
	Chicken ovalbumin upstream promotor-transcription factor β	COUP-TFβ	Orphan
	Chicken ovalbumin upstream promotor-transcription factor γ	COUP-TFγ	Orphan
3A	Estrogen receptor-α	ERα	Estrogens

Subfamily	Name	Abbreviation	Ligand
	Estrogen receptor-β	ERβ	Estrogens
3B	Estrogen-related receptor-α	ERRα	Orphan
	Estrogen-related receptor-β	ERRβ	Orphan
	Estrogen-related receptor-γ	ERRγ	Orphan
3C	Androgen receptor	AR	Androgens
	Glucocorticoid receptor	GR	Gluc
	Mineralcorticoid receptor	MR	Gluco- and mineralcorticoids
4A	Nerve growth factor 1B	NGF1-B	Orphan
	Nurr-related factor 1	NURR1	Unsaturated fatty acids
	Neuron-derived orphan receptor 1	NOR-1	Orphan
5A	Steroidogenic factor 1	SF-1	Phospholipids
	Liver receptor homolog-1	LRH-1	Phospholipids
6A	Germ cell nuclear factor	GCNF	Orphan

1.2 Retinoic acid receptor-related orphan receptors (RORs)

The retinoic acid receptor-related orphan receptors (RORs) form the NR1F subfamily of nuclear receptors (see Table 1) and include the three members RORα, RORβ and RORγ, which are encoded by the genes RORA, RORB, and RORC, respectively (or NR1F1-3)[4,5] They were named based on their sequence similarity to retinoic acid receptors (RARs) and retinoid X receptors (RXRs) [4]. Although oxysterols have been suggested as potential endogenous ligands, their role is still not fully established, and RORs continue to be classified as orphan nuclear receptors [5].

Each of these genes can generate multiple receptor isoforms, mainly through alternative promoter usage and splicing. These isoforms mainly differ in their N-terminal A/B domain, while the remaining regions are largely conserved [4,13]. The three ROR subtypes, RORα, RORβ, and RORγ, were identified in the early 1990s, with RORα being the first characterized member [14]. Each receptor displays a distinct tissue-specific expression pattern. RORα is broadly expressed in various peripheral tissues, including liver, skeletal

muscle, lung, kidney, skin, brain, thymus and adipose tissue [4]. In contrast, RORβ expression is largely restricted to the central nervous system, particularly in regions such as the brain, retina, and pineal gland; however, RORβ has also been detected in osteoblasts and human bone tissue [8]. RORγ is found in liver, skeletal muscle, adipose tissue and kidney. However, the isoform RORγt, which varies only in the first 100 nucleotides of the N-terminal region, is specifically expressed in immune cells, including thymocytes and TH17 cells [4,15,16].

1.2.1 Transcriptional Regulation and Ligands of RORs

RORs regulate gene expression by binding as monomers to specific DNA motifs in target gene promoters. These motifs are referred to as ROR response elements (ROREs) and are commonly described by the consensus sequence TAAA/TNTAGGTCA [4]. Upon binding to response elements in target gene promoters, RORs exhibit constitutive activity and recruit coactivators independently of ligand binding, resulting in ligand-independent transcriptional activation [4,17]. Consequently, in addition to agonists and antagonists, inverse agonists can reduce receptor activity below its constitutive basal levels [4,18].

Ligand-dependent regulation occurs within the ligand-binding domain (LBD). Ligand binding induces conformational changes, particularly involving helix 12, which influence the recruitment of transcriptional coregulators [17–19]. Coactivator recruitment promotes transcriptional activation, while inverse agonist-induced recruitment of corepressors leads to reduced target gene expression [17,18]. ROR-mediated transcription is additionally counterbalanced by REV-ERB receptors, which recognize similar DNA response elements but act as transcriptional repressors through corepressor recruitment [4,18].

1.2.2 Endogenous and synthetic ligands

As mentioned before, RORs are constitutively active, meaning they can drive the expression of target genes even without ligand binding. Therefore, ligands may act as antagonists or inverse agonists, reducing transcription below basal levels [17]. Given the central role of ligand binding in regulating ROR activity, numerous endogenous and exogenous compounds have been identified as modulators of these receptors. The following section summarizes selected examples of endogenous, synthetic, and natural

ROR ligands. An overview of selected ROR ligands, their chemical structures, and reported receptor targets is provided in Table 2.

A subtype-specific pattern is seen among endogenous ligands. RORβ differs from RORα and RORγ in both tissue distribution and function and has been reported to bind distinct ligands such as stearic acid and all-trans retinoic acid (ATRA) [17,18,20]. However, stearic acid is unlikely to represent a physiological activating ligand of RORβ, since it did not activate RORβ in a cell-based reporter assay and showed only partial occupancy of the ligand-binding pocket. Therefore, stearic acid has been suggested to act mainly as a stabilizer of the RORβ ligand-binding domain rather than as a true activating ligand [21]. In contrast, RORα and RORγ share related sterol- and cholesterol-derived ligands, including 7α/7β-hydroxycholesterol, 7-ketocholesterol, (24R/S)-hydroxycholesterol and 24,25-epoxycholesterol [17,22].

The identification of these endogenous ligands enabled the development of synthetic ROR modulators. The compound T0901317, originally described as an LXR/FXR agonist[23], was later identified as an inverse agonist of RORα and RORγ and served as a starting point for the development of ROR-targeted ligands [24]. Based on this scaffold, several synthetic compounds were developed, including SR1078, an agonist of RORα and RORγ [25] and SR1001, an inverse agonist of both receptors [26]. In addition, SR2211 is a more selective RORγ inverse agonist [27]. SR20156, which was used as a positive control in this study, showed potent inverse agonistic activity on RORβ (IC_{50} < 0.010 μM). In the same study, weaker activity on RORγ was reported (IC_{50} > 3.0 μM), indicating selectivity for RORβ over RORγ.[28] Furthermore, all-trans retinoic acid (ATRA) has also been described as an inhibitor of RORβ [20].

In parallel, several natural products that modulate ROR activity have been identified. Digoxin and digitoxin act as inverse agonists of RORγ, while diosgenin inhibits both RORα and RORγ. Ursolic acid also functions as a RORγ inverse agonist and suppresses TH17 differentiation and IL-17 expression, although its therapeutic use is limited by off-target effects [15,29]. In contrast, 25-hydroxycholesterol acts as an agonist of RORγ [18].

Table 2. **Selected ROR ligands** (created with the assistance of ChemDraw)

Name	Chemical Structure	Target
Cholesterol	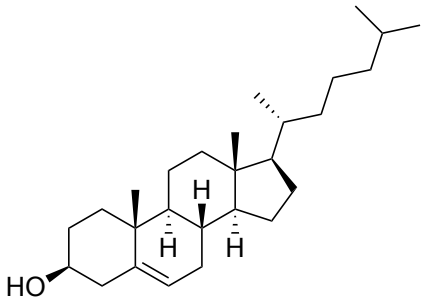	RORα agonist
25-hydroxycholesterol	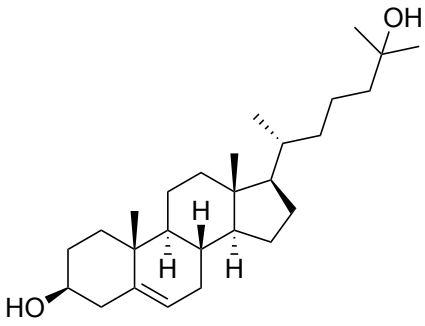	RORγ agonist
Ursolic acid	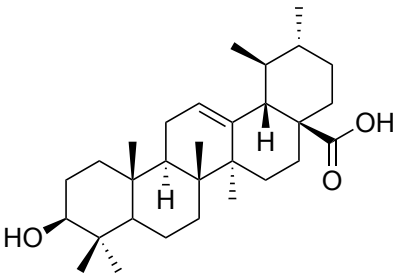	RORγ (t) inverse agonist
Digoxin	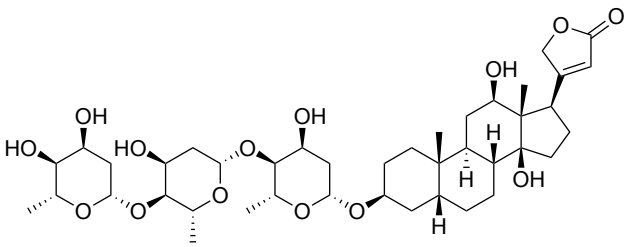	RORγ (t) inverse agonist

Digitoxin	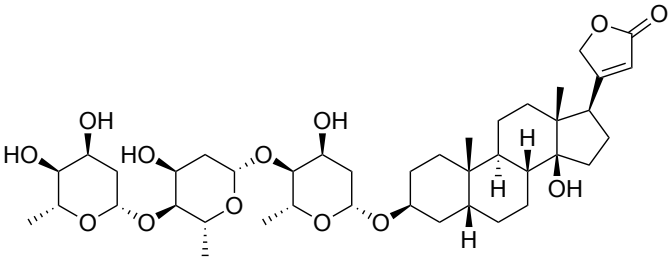	RORγ (t) inverse agonist
Diosgenin	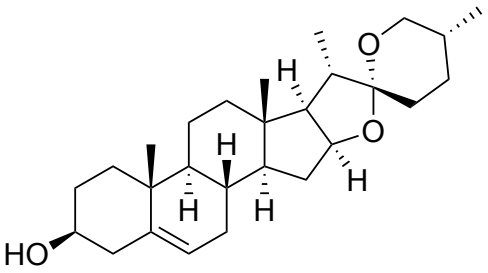	RORα inverse agonist, RORγ inverse agonist
T0901317	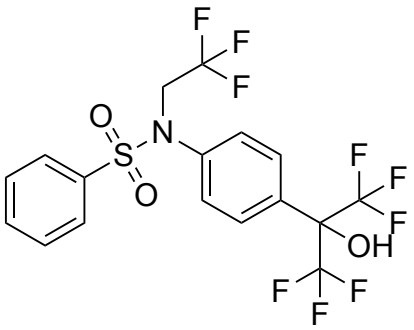	LXR/FXR agonist, RORα inverse agonist, RORγ inverse agonist
SR1001	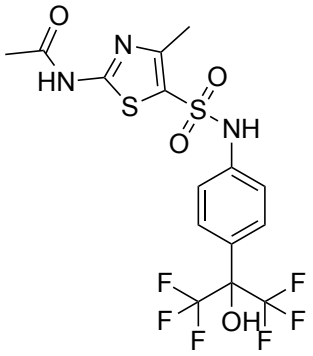	RORα inverse agonist, RORγ inverse agonist
SR2211	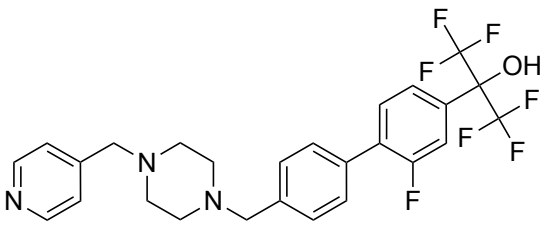	RORγ inverse agonist

SR 20156	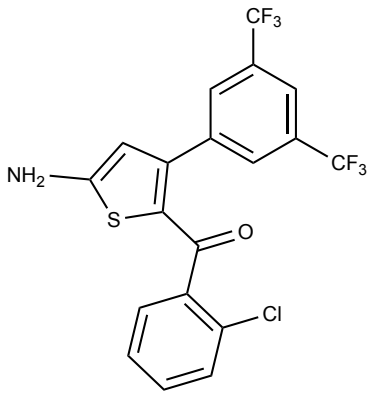	RORβ inverse agonist, RORγ (t) inverse agonist

1.3 Biological and Disease-Related Functions of RORs

RORs play important roles in circadian rhythm regulation, metabolic processes, and immune function and have been implicated in a variety of disease-related processes[17]. While RORα and RORγ have been extensively studied in these contexts, RORβ remains less well characterized.[30]

1.3.1 Roles of RORα and RORγ in Immune, Circadian and Metabolic Regulation

RORγt is particularly relevant in immune regulation. CD4+ T cells were initially classified mainly into TH1 and TH2 subsets, but the discovery of TH17 cells revealed an additional pathway involved in host defense and autoimmune inflammation [17]. TH17 differentiation from naïve $CD4^+$ T cells is induced by cytokines such as IL-6 and transforming growth factor beta (TGF-β) and depends on activation of the transcription factor STAT3 [31]. RORα and in particular, RORγt contribute to this process and drive TH17 cell development[16]. IL-23 further stabilizes the TH17 phenotype and enhances its pathogenic potential [15,32]. TH17 cells produce pro-inflammatory cytokines, including IL-17A, IL-17F, IL-21, and IL-22. These cytokines contribute to immune defense against extracellular pathogens but are also associated with autoimmune diseases such as multiple sclerosis, rheumatoid arthritis, and psoriasis [17,32,33]. Genetic ablation of RORγt, particularly in combination with loss of RORα, impairs TH17 differentiation and reduces autoimmune disease development in experimental models [16].

Besides their role in immune regulation, RORs are also involved in the control of circadian rhythm. RORα contributes to the regulation of the circadian clock, a transcriptional-translational feedback system that controls numerous physiological processes, including the sleep-wake cycle, feeding behavior, metabolism, body temperature, blood pressure, and renal function. In mammals, the central circadian clock is located in the *Nucleus suprachiasmaticus* of the hypothalamus [17]. This molecular clock is driven by interconnected transcriptional-translational feedback loops, in which the transcription factors BMAL1 and CLOCK form heterodimers that act as the positive regulatory arm by inducing the expression of period (PER1, PER2 and PER3) and cryptochrome (CRY1 and CRY2) genes [17,18]. The resulting PER and CRY proteins constitute the negative arm, by inhibiting BMAL1-CLOCK activity and thereby suppress their own transcription [17]. RORα contributes to the regulation of this system by positively modulating BMAL1 expression, further supporting the stability of the circadian clock. RORs and REV-ERBs control BMAL1 expression in an opposing manner, with ROR enhancing and REV-ERBα suppressing its transcription. Both receptors are expressed in a rhythmic manner, alternating approximately every 12 hours [17,18].

In addition to immune and circadian regulation, RORα and RORγ are involved in metabolic processes. Studies using genetic models showed that RORα deficiency is associated with reduced plasma lipid levels, including cholesterol, HDL, and triglycerides, as well as altered expression of genes involved in lipid synthesis, transport, oxidative metabolism, and gluconeogenesis [17,18,34]. These mice are resistant to weight gain and hepatic steatosis, particularly under high-fat diet conditions, and show altered expression of genes involved in oxidative metabolism. RORα also regulates genes involved in bile acid synthesis and gluconeogenesis, such as Cyp7b1 and G6pase, and has been linked to the control of FGF21 expression, highlighting its role in hepatic metabolism and glucose homeostasis [34,35]. In contrast, RORγ-deficient mice display largely normal serum lipid profiles but show reduced blood glucose levels under obese conditions [34,36]. RORγ has been implicated in adipogenesis and insulin sensitivity, as its absence leads to smaller, more insulin-sensitive adipocytes and protection against obesity-induced metabolic dysfunction [36]. Although RORα and RORγ share some overlapping functions, they also exhibit distinct roles in glucose homeostasis and adipose tissue biology, indicating both functional redundancy and specialization within this receptor family [18,34].

1.3.2 RORβ: Neuronal Functions and Emerging Roles in Bone Biology

Compared to RORα and RORγ, the functional characterization of RORβ is more limited [6,18]. Whereas RORα is closely associated with metabolic regulation and circadian rhythm and RORγ plays a central role in immune responses, current evidence suggests that RORβ is primarily involved in neuronal development, sensory processing, and possibly circadian regulation [6,18,37]. Its role in metabolic and immunological processes remains less well established. RORβ is predominantly expressed in the central nervous system, particularly in the retina and brain regions involved in circadian regulation. This expression pattern suggests a role in visual function and circadian timing, which is supported by findings that RORβ deficiency leads to retinal degeneration and altered circadian rhythmicity [6,18,38]. Moreover, RORβ has been implicated in epileptic and neurodevelopmental disorders, as well as in certain psychiatric conditions, further highlighting its role in neuronal differentiation and function [7]. More recently, RORβ has been linked to bone biology. As a transcription factor, it inhibits Runx2-mediated gene activation and thereby restricts osteoblast differentiation. This is illustrated in Figure 3, which shows that Runx2 promotes the differentiation of mesenchymal stem cells toward osteoblasts and supports bone formation, while RORβ acts as a negative regulator of Runx2-dependent osteoblast differentiation. Although RORβ was initially considered to be largely restricted to the retina and brain, its expression has also been detected in osteoblast cell lines and in bone tissue from mice and humans [8] RORβ levels are elevated in immature osteoblasts and decline during differentiation, while sustained expression also impairs mineralization. Increased RORβ expression has additionally been observed in human bone biopsies from post-menopausal women as well as in osteoblast precursors from aged, osteoporotic mice, indicating a potential role in age-related bone loss. Although RORβ has been shown to influence several osteogenic pathways, its complete target network in bone cells remains incompletely understood [8].

Despite growing evidence linking RORβ to neuronal function, circadian regulation[6], and bone biology [8], no fully selective RORβ modulator has been established so far [6,17]. In particular, the effects of natural products and their derivatives on RORβ remain poorly understood. Since natural compounds are an important source for drug discovery,

identifying new RORβ modulators may help to further clarify the physiological role and therapeutic potential of this receptor [15,17].

In conclusion, RORβ appears to function as a nuclear receptor with predominant roles in the central nervous system and growing relevance in bone biology [6,8,37]. However, its precise physiological functions and therapeutic potential remain insufficiently understood and require further investigation [18].

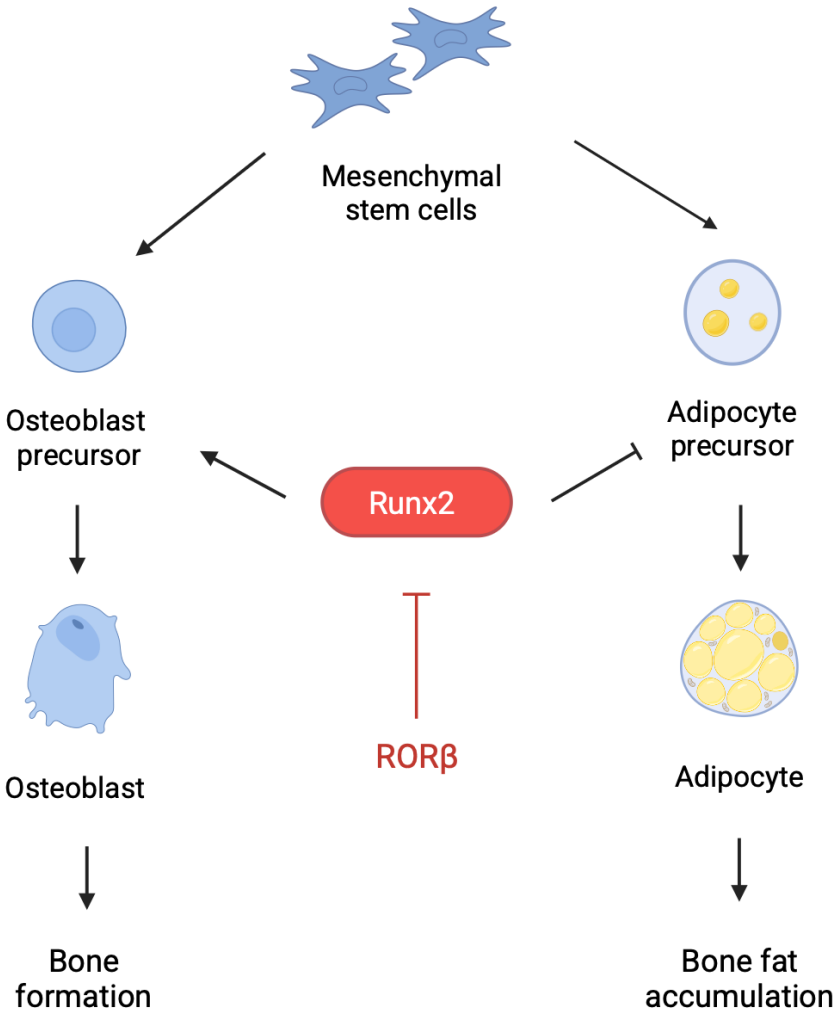

Figure 3. **RORβ inhibits osteoblast formation via RUNx2 inhibition:** Runx2 promotes osteoblast differentiation and bone formation from mesenchymal stem cells while inhibiting adipocyte differentiation and bone fat accumulation. RORβ acts as a negative regulator of Runx2. Adapted from [38] created with BioRender.com.

2 Aim of the study

RORβ remains less well characterized than other members of the ROR family. Therefore, the identification of additional RORβ ligands may contribute to a better understanding of its biological function and potential therapeutic relevance [7,8]. The aim of this thesis was to identify novel ligands of RORβ.

To achieve this, selected natural products and derivatives from in-house collections and from collaborative compound collections provided through different cooperation partners, as described in Section 3.2, were screened using luciferase reporter gene assays.

Overall, this screening identified several candidate RORβ modulators that warrant further investigation.

3 MATERIAL AND METHODS

3.1 Cell culture

All experiments were conducted under sterile conditions using the laminar airflow cabinet HERAsafe® to prevent contamination. Cells were kept in a humidified HERAcell® 150 incubator at 37°C and 5% CO_2. An overview of the devices used for cell culture experiments is provided in Table 3, while the compositions of the media and other materials used are summarized in Table 4.

Table 3. **Devices used in cell culture**

Name	Provider
Biological Safety Cabinets Herasafe™	Thermo Fisher Scientific Inc. (Waltham, USA)
Heracell™ 150 Incubator	Thermo Fisher Scientific Inc. (Waltham, USA)
VI-Cell™ XR Cell Viability Analyzer	Beckmann Coulter (Brea, USA)
Centrifuge Haraeus™ Multifuge 1 S-R	Thermo Fisher Scientific Inc. (Waltham, CA, USA)
Digital Microplate Shaker	Thermo Fisher Scientific Inc. (Waltham, CA, USA)
Light Microscope Olympus CKX31	Olympus Europa GmbH (Hamburg, DE)
VM-3000 Mini Vortexer	VWR International (Radnor, PA, USA)
Julabo ® SW23 shaking water bath	Julabo GmbH (Seelbach, DE)

Table 4. **Materials used in cell culture experiments**

Name	Ingredients	Amount	Provider
Complete medium	DMEM with 4.5 g/l glucose	500 ml	Sigma-Aldrich (St. Louis, US)
	2 mM glutamine solution	5 ml	Lonza (Basel, CH)
	Penicillin	5 ml (100 U/ml)	Lonza (Basel, CH)
	Streptomycin	5 ml (100 µg/ml)	Lonza (Basel, CH)
	FBS	50 ml (10%)	Gibco (Lofer, AT)
Stripped medium	DMEM with 4.5 g/l glucose	500 ml	Lonza (Basel, CH)
	2 mM glutamine solution	5 ml	Lonza (Basel, CH)
	Penicillin	5 ml (100 U/ml)	Lonza (Basel, CH)
	Streptomycin	5 ml (100 µg/ml)	Lonza (Basel, CH)
	Charcoal-stripped FBS	25 ml (5%)	Gibco (Lofer, AT)

Stripped medium without phenol red	DMEM with 4.5 g/l glucose 2 mM glutamine solution Penicillin Streptomycin Charcoal-stripped FBS	500 ml 5 ml 5 ml (100 U/ml) 5 ml (100 µg/ml) 25 ml (5%)	Corning Optical Communications GmbH & Co. KG (Berlin, Germany Lonza (Basel, CH) Lonza (Basel, CH) Lonza (Basel, CH) Gibco (Lofer, AT)
PBS pH 7.4	Nacl Na_2HPO_4 KH_2PO_4 ddH_{2O}	36.0 g 7.4 g 2.15 g	Carl-Roth (Karlsruhe, DE) Carl-Roth (Karlsruhe, DE) Carl-Roth (Karlsruhe, DE)
Trypsin/EDTA solution	Trypsin (1:250) Na_2-EDTA PBS	0.5 g 0.2 g 1000 ml	Gibco (Lofer, AT) Gibco (Lofer, AT)

3.1.1 HEK 293 cells

Human embryonic kidney 293 cells obtained from American Type Culture Collection (ATCC, Manassas, US), which grow adherently, were used for luciferase and resazurin assays.

Cells were maintained in 175 cm^2 culture flasks (Sarstedt AG & Co.KG, Nümbrecht, Germany) containing complete Dulbecco's Modified Eagle's Medium (DMEM), supplemented with 4.5 g/l glucose. The composition of the cell culture medium is summarized in Table 3. Complete medium was prepared by adding 2 mM glutamine solution, 100 U/ml penicillin and 100 µg/ml streptomycin, and 10% fetal bovine serum (FBS). For experiments, charcoal-stripped medium was used, in which FBS was replaced with 5% charcoal-stripped FBS. Media were stored at 4 °C and used within one month after addition of nutrients and antibiotics.

HEK293 cells were subcultured on Monday, Wednesday, and Friday to maintain sub-confluent cultures. Phosphate-buffered saline, growth medium, and trypsin/EDTA solution were prewarmed at 37 °C for approximately 30 minutes prior to cell splitting. Cell density and contamination were assessed using an Olympus CKX31 light microscope. Upon confirming the absence of contamination, the old medium was disposed of, and cells were washed with 10 ml of phosphate-buffered saline. Following the removal of the washing solution, 3 ml of Trypsin/EDTA solution were added, and flasks were then

incubated at 37 °C and 5% CO_2 for two minutes to detach adherent cells. The trypsinization process was terminated by addition of complete DMEM in a volume at least twice that of the applied Trypsin/EDTA solution, and residual adherent cells were collected by gentle washing. Cell number and viability were determined using the Vi-Cell™ XR Cell Viability Analyzer. For cultivation, between 6×10^6 and 8×10^6 cells were seeded and incubated at 37 °C and 5% CO_2. The HEK293 cells were cultivated up to a passage number of 30, after which they were discarded.

3.2 Compounds

The compounds used in this study originated from several sources. The focus was on compounds provided by Karel Šmejkal (Faculty of Pharmacy, Masaryk University) and Franz Bracher (Department of Pharmacy – Center for Drug Research, Ludwig Maximilian University of Munich), as well as a series of phytoecdysteroids provided by Attila Hunyadi (Institute of Pharmacognosy, University of Szeged).

Additional compounds included selected in-house compounds, anti-inflammatory in-house compounds, and compounds from the in-house database “Drugs from Nature Targeting Inflammation” (DNTI). The DNTI database comprises plant extracts, mixtures, and isolated compounds previously screened for anti-inflammatory effects related to the cardiovascular system. It was established between 2008 and 2014 as part of a collaborative project involving eight research groups from six Austrian universities [39].

Powdered compounds were weighed and dissolved in dimethyl sulfoxide (DMSO). Stock solutions were prepared at concentrations ranging from 0.001 mM to 100 mM using the respective solvent and stored at −20 °C. For all experiments, these stock solutions were further diluted 1:1000 in stripped medium to obtain final concentrations ranging from 0.001 µM to 100 µM.

3.3 Luciferase assay

3.3.1 Background information

The luciferase reporter assay is a widely used reporter gene assay for high-throughput screening. It allows changes in transcription factor activity or promoter activity to be monitored by measuring luciferase-driven light emission (Fig. 4). In this case, it was used to evaluate the activity of a test substance on the nuclear receptor RORβ [40].

For initial screening, a mammalian one-hybrid Gal4 luciferase reporter assay was predominantly used. In this system, the ligand-binding domain (LBD) of RORβ is fused to the DNA-binding domain (DBD) of the yeast transcription factor Gal4. The GAL4 DBD binds to upstream activating sequences (UAS) to drive the expression of a luciferase reporter gene. Receptor activity is further modulated by ligand binding to the RORβ LBD, where agonists promote transcriptional activation and increase luciferase expression. Inverse agonists, in contrast, suppress receptor activity by reducing transcriptional activation, leading to decreased luciferase expression. The luciferase enzyme subsequently catalyzes the conversion of luciferin to oxyluciferin, resulting in light emission that can be quantified using a plate reader. Compounds showing agonistic or inverse agonistic activity in this Gal-4 assay were further evaluated using a RORE-dependent transactivation assay. Specifically, compounds showing a Fold Activation (FA) of < 0.70 or > 1.5 were selected for further testing. In contrast to the Gal4 system, the RORE-dependent transactivation assay employs the full-length (wild-type) RORβ receptor containing both its native DBD and LBD. In this case, receptor activity is measured via ROR response elements (ROREs) coupled to a luciferase reporter gene. This setup allows assessment of compound effects on RORβ in a more physiological context [41–43]. Active compounds from the GAL4-RORβ assay were confirmed in this full-length

RORβ assay and subsequently tested in GAL4-RORγ, full-length RORγ, and GAL4-RORα assays to assess selectivity.

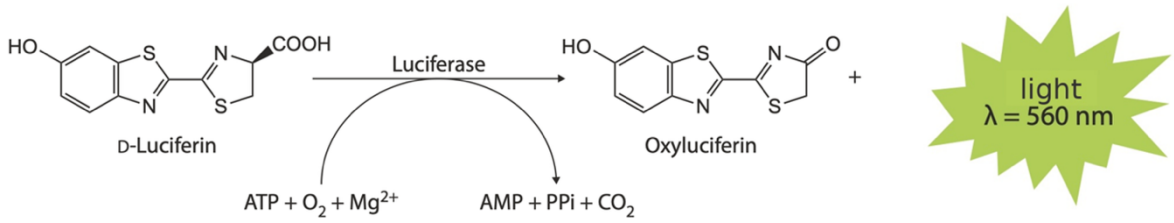

Figure 4. **Luciferase reaction.** The enzyme luciferase converts D-Luciferin into oxyluciferin, after which light is emitted. The reaction also requires other components such as magnesium and ATP. [42]

3.3.2 Seeding of the cells

8×10^6 HEK293 cells were seeded into a 150 mm dish. For each 96 well plate, a 150 mm dish was prepared for transfection, and one additional 150 mm dish containing untransfected cells was used as a shared control for multiple plates.

3.3.3 Transfection

Approximately five hours later, HEK293 cells were transfected using the calcium phosphate precipitation method [44]. Under a sterile hood, all reagents and plasmid DNAs were combined in reaction tubes to prepare the transfection mixture, which was kept at room temperature for 20 minutes before use. Subsequently, 1,500 µl of the mixture were carefully added dropwise to each 150 mm culture dish. This study utilized three plasmids, including a reporter plasmid with the luciferase gene controlled by Gal4-UAS elements, an expression plasmid encoding RORβ fused to the Gal4 DNA-binding domain, and an eGFP plasmid serving as a transfection efficiency control (Table 5). The transfected culture dishes were then incubated overnight at 37°C with 5% CO_2. After overnight transfection, the cells were examined under a microscope, washed once with PBS, and the medium was replaced with fresh complete DMEM.

Table 5. **Plasmids and transfection mixture**

	Amount	Provider
RORβ-GAL4 or Full-length RORβ	5 µg	Laura Solt, Ph.D. (Florida, USA)

UAS (MH1000) 4x LUC	5 µg	Salk Institute for Biological Studies (CA, USA)
peGFP-N1	3 µg	Sigma-Aldrich (St. Louis, US)
2x HBS (hepes-buffered saline)	750 µl	Carl Roth (Karlsruhe, DE)
$CaCl_2$ 2M	94 µl	Carl Roth (Karlsruhe, DE)
ddH_2O	ad 1500 µl	

3.3.4 Dilution and compound treatment

The test samples were diluted 1:250 in stripped DMEM. Then, 50 µl of the diluted compounds were added in quadruplicate to the designated wells. For cell preparation, the old medium was removed, and the dishes were washed with 10 ml PBS. Cells were detached using trypsin/EDTA, and trypsinization was stopped by adding complete DMEM, followed by thorough resuspension to detach remaining adherent cells. The suspension was transferred into 50 ml tubes and centrifuged at 410 × g for 4 minutes. After removal of the supernatant, the cell pellets were resuspended in stripped DMEM, and a defined aliquot was used for cell counting and viability assessment using the Vi-Cell™ XR Cell Viability Analyzer. Based on these results, the suspensions were adjusted to a final density of 50,000 cells per well. Finally, 150 µl of the diluted transfected cell suspension were added to the designated wells, resulting in a total volume of 200 µl per well and a final compound dilution of 1:1000. Control wells were filled with 200 µl of non-transfected cells. The plates were incubated at 37 °C and 5% CO_2 for 18 hours.

3.3.5 Examination

After 18 hours of incubation, the cells were examined using the fluorescence microscope Olympus BX51 to assess transfection efficiency, cell viability, and potential signs of toxicity. Following this evaluation, the medium was completely removed from all wells using a vacuum pump, after which the plates were stored at −80 °C for at least one hour and up to one week.

3.3.6 Measurement

Immediately prior to cell lysis, the lysis buffer was prepared as indicated in Table 6. Subsequently, 50 µl of the lysis buffer were added to each well, and the plate was shaken on a Digital Microplate Shaker for 10 minutes. After lysis, 40 µl of the cell lysate were transferred to a black 96-well plate and evenly distributed by gentle tapping. Fluorescence and luminescence were then measured using a Tecan Spark® Microplate Reader, with ATP and luciferin injected into the respective wells via injector A and B, using the instrument settings summarized in Table 6 and Table 7.

Table 6. ***Components of the 1x lysis buffer***

Name	Amount	Provider
ddH_2O	4.8 ml	
5× lysis buffer	1.2 ml	Promega (Madison, WI, USA)
Dithiothreitol (DTT)	6 µl	Sigma-Aldrich (St. Louis, MO, USA)
Coenzyme A (CoA) trilithium salt	2 µl	Sigma-Aldrich (St. Louis, MO, USA)

Table 7. **Instrument settings for luminescence measurements**

Plate	[GRE96fb_chimney] – Greiner 96 Flat Black [GRE96fb_chimney]
Lid lifter	No lid
Humidity Cassette	No humidity cassette
Smooth mode	Selected
Name	GRE96fb_chimney
Plate layout	
Plate area	A1-H12
Mode	Well
Injector A	
Volume	50 µl
Speed	150 µl/sec
Refill speed	100 µl/sec
Refill mode	Standard
Injector B	
Volume	50 µl

Speed	150 µl/sec
Refill speed	100 µl/sec
Refill mode	Standard
Mode	Luminescence
Name	Luminescence
Attenuation	None
Settle time	50 ms
Integration time	2000 ms
Output	Counts / s
Part of plate	A1-H12

Table 8. **Instrument settings for fluorescence measurements**

Parameter	Setting
Plate	Greiner 96 Flat Bottom Black Polystyrol (GRE96fb_chimney.pdfx)
Mode	Fluorescence Top Reading
Excitation wavelength	485 nm
Emission wavelength	520 nm
Excitation bandwidth	9 nm
Emission bandwidth	20 nm
Gain	Optimal (100%)
Number of flashes	25
Integration time	1000 µs
Lag time	0 µs
Settle time	0 ms
Z-position (manual)	20000 µm

Table 9. **Substrates used for measurements**

Name	Ingredients	Provider
Adenosin-5' triphosphate disodium salt (ATP)	2 mM tricine (pH 7.8) 21.5 mM $MgCl_2$ 3.8 mM ATP	Sigma-Aldrich (St. Louis, MO, USA)
D-Luciferin (sodium salt)	21 mM tricine (pH 7.8) 32 mg/ml luciferin	Synchem (Elk grove Village, US)

3.3.7 Data analysis

Data analysis was performed using Microsoft Office Excel (Microsoft Corporation) and GraphPad Prism 11.0.2. In Excel, mean values of compounds measured in quadruplicates were calculated. Background luminescence and fluorescence from untransfected cells were subtracted, after which luminescence signals were normalized to fluorescence and further normalized to the solvent control (DMSO), with results expressed as fold activation relative to DMSO. In addition, normalized fluorescence values were used as a quality control parameter. Conditions with fluorescence values below 0.70 relative to the solvent control were indicated by red bars in the figures. [45] Experiments conducted for screening purposes were performed once, whereas all other experiments were carried out in three biological replicates. Data are presented as mean values ± standard deviation. GraphPad Prism was used for statistical analysis, IC_{50} determination, and generation of concentration-response curves. Concentration-response data from compounds tested at different concentrations were plotted on a logarithmic scale to obtain sigmoidal curves. For concentration-response curve fitting and calculation of IC_{50} or EC_{50} values, nonlinear regression was performed in GraphPad Prism using the function “log(inhibitor) vs. response – three parameters” or the corresponding agonist-response model, depending on the direction of the compound effect. One-way analysis of variance (ANOVA) followed by Dunnett’s post-hoc test was applied, with p-values < 0.05 considered statistically significant.

3.4 Resazurin conversion assay

The resazurin assay is a simple and efficient method to evaluate cell viability and cytotoxicity of test compounds [46]. Resazurin is a blue, cell-permeable redox dye that is taken up by cells and reduced to the pink, fluorescent compound resorufin only in metabolically active cells (Fig. 5). This conversion is accompanied by a visible color change from blue to pink [47]. The amount of resorufin can be quantified by fluorescence measurement, with the signal directly proportional to the number of viable cells [46,48].

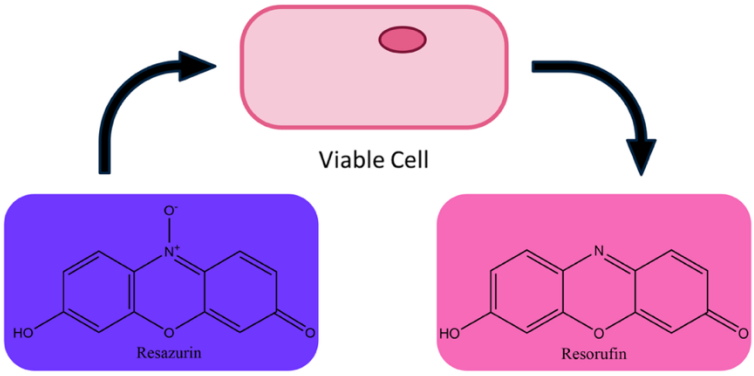

Figure 5. **Resazurin reduction (Illustration created with BioRender.com.** Resazurin is reduced to resorufin by metabolically active cells, resulting in a measurable fluorescence signal that reflects cellular metabolic activity and viability.

3.4.1 Dilution of samples and treatment of cells

To ensure comparable conditions and incubation times, the resazurin assay was conducted in parallel with the luciferase assay. For this purpose, compounds previously diluted 1:250 in stripped medium were pipetted into a 96-well plate (50 µl per well). Untransfected HEK293 cells, prepared as described for the luciferase assay, were then added (150 µl per well; 50,000 cells per well), resulting in a total volume of 200 µl per well. 50 µg/ml Digitonin served as a cytotoxic positive control.[46] The plates were then incubated at 37 °C and 5% CO_2 for 18 hours.

3.4.2 Preparation of resazurin stock

On the following day, a resazurin stock solution was prepared by dissolving resazurin sodium salt (Sigma-Aldrich) in PBS to a final concentration of 0.1 mg/ml. The solution was mixed thoroughly and sterilized by filtration through a 0.2 µm syringe filter into a 50 ml tube. The stock solution was stored at 4 °C and used within four weeks. Prior to use, it was diluted 1:10 with stripped medium without phenol red to obtain a working solution at a final concentration of 10 µg/ml.

3.4.3 Measurement

Following the 18-hour incubation period, the culture medium was carefully removed from each well and 150 µl of stripped medium containing 10 µg/ml resazurin was added. Following the 18-hour incubation, the medium was gently removed from each well and replaced with 150 µl of stripped medium containing 10 µg/ml resazurin. The plates were

returned to the incubator at 37 °C and 5% CO_2 and fluorescence was measured after 4 hours using a Tecan Spark® Microplate Reader (excitation: 535 nm; emission: 590 nm), using the instrument settings summarized in Table 10.

Table 10. **Instrument settings for resazurin measurement**

Plate	Greiner 96 Flat Bottom Transparent Polystyrol [GRE96ft.pdfx]
Mode	Fluorescence Top Reading
Excitation Wavelength	535 nm
Emission Wavelength	590 nm
Excitation Bandwidth	9 nm
Emission Bandwidth	20 nm
Gain	Optimal (100%)
Number of Flashes	25
Integration Time	40 µs
Lag Time	0 µs
Settle Time	0 ms
Z-Position (Manual)	20000 µm

3.4.4 Data analysis

Data from the resazurin conversion assays were analyzed using Microsoft Office Excel and GraphPad Prism 11.0.2. Measurements were performed in quadruplicates, and each experiment was conducted in three biological replicates. Mean values and standard deviations of relative fluorescence units were calculated in Excel and normalized to the solvent control (DMSO). (Compounds resulting in cell viability greater than 75% relative to the control were considered non-toxic.) Relative resazurin conversion was expressed as a percentage of the control, with the negative control set to 100%, and compounds with values below 75% were considered cytotoxic, whereas those above 75% were regarded as non-toxic. GraphPad Prism was used for statistical analysis and generation of final figures.

4 Results

To identify potential modulators of RORβ, a luciferase reporter gene assay was established in HEK293 cells. After evaluation of suitable positive controls, SR20156 was selected as a positive control for inverse agonistic activity [28]. While SR1078 has been reported as a synthetic agonist for RORα and RORγ [25] no established positive control for agonistic activity was available for RORβ in this assay setting. Therefore, the assay was validated by determining whether reduced transactivation activity could be reliably detected using SR20156 as reference inverse agonist. The assay was then used to screen compounds from different in-house and collaborative collections. Specifically, compounds showing a Fold Activation (FA) of < 0.70 or > 1.5 were selected for further testing. These compounds were further evaluated in follow-up assays to assess concentration-dependent effects, potential receptor selectivity, reporter-associated off-target effects, and effects on cell viability. Based on these results, the following section focuses on SR20156 as suitable positive control, the structurally related compounds epicorosolic acid (SD5) and corosolic acid (SD2), and the phytoecdysteroid derivative CR27.

4.1 Selecting a suitable positive control for the Gal4-RORβ luciferase reporter gene assay using SR20156

Although ATRA has been described as a ligand of RORβ [20], its use as a positive control compound is limited by its light sensitivity, instability under non-protected conditions, and lack of receptor selectivity, as it can also bind RARs and RXRs[28], and has also been reported to inhibit RORγ [20]. In contrast, SR20156 was synthesized and reported by Doebelin et al. as a RORβ modulator derived from structural modification of a dual RORβ/RORγ inverse agonist, with the aim of improving selectivity toward RORβ [28]. Therefore, SR20156 (Fig. 6) was used as the reference inverse agonist for assay establishment.

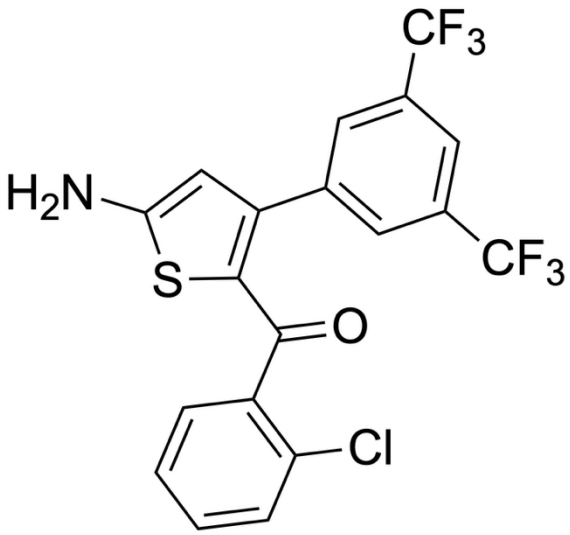

Figure 6. **Chemical structure of SR20156** adapted from [19], created with the assistance of Chemdraw.

SR20156 reduced Gal4-RORβ-dependent transactivation activity in a concentration-dependent manner in the tested concentration range of 1 nM-30 µM (Figs.7 and 8). In the bar graph, SR20156 showed the strongest reduction in Gal4-RORβ transactivation activity at 30 µM. The corresponding fluorescence value was below the predefined threshold of 0.70 relative to the solvent control, which is indicated by the red bar in the figure [45]. This threshold was used to identify conditions in which reduced fluorescence may indicate reduced cell metabolic activity, altered cell number, or weaker assay performance, and therefore reduced reliability of the corresponding luciferase reporter readout. At lower concentrations, the FA gradually approached the level of the solvent control. Nonlinear

regression analysis resulted in an IC_{50} value of 3.56 µM. The corresponding concentration-response curve showed a clear sigmoidal trend, supporting the use of SR20156 as reference inverse agonist in the established assay. Together, these results confirmed that the Gal4-RORβ luciferase reporter gene assay was suitable for detecting concentration-dependent decreases in RORβ activity.

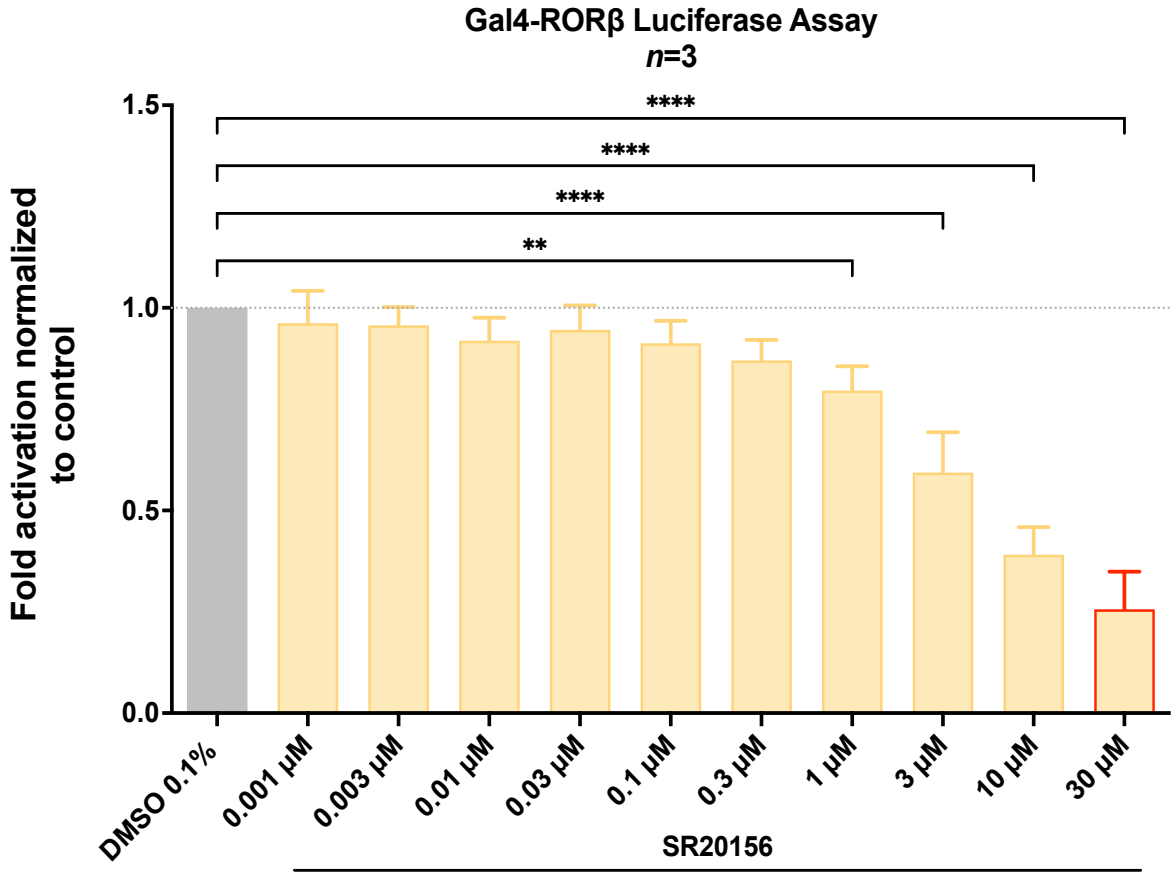

Figure 7. **Luciferase assay results for SR20156.** HEK293 cells were transiently transfected with the Gal4-RORβ reporter system and eGFP as an internal control, followed by treatment with SR20156 for 18 h. Luminescence signals were normalized to the corresponding fluorescence signals and subsequently to the solvent control DMSO 0.1%. Values are shown as FA relative to the solvent control and represent mean ± SD of three biological replicates measured in technical quadruplicates. A red bar indicates that the corresponding RFU value was below the predefined threshold of 0.70 relative to the solvent control at the respective concentration. Statistical analysis was performed using one-way ANOVA followed by Dunnett's post hoc test. ****$p \leq 0.0001$, ***$p \leq 0.001$, **$p \leq 0.01$, *$p \leq 0.05$. Absence of significance indication denotes no statistically significant difference compared with the solvent control DMSO 0.1%.

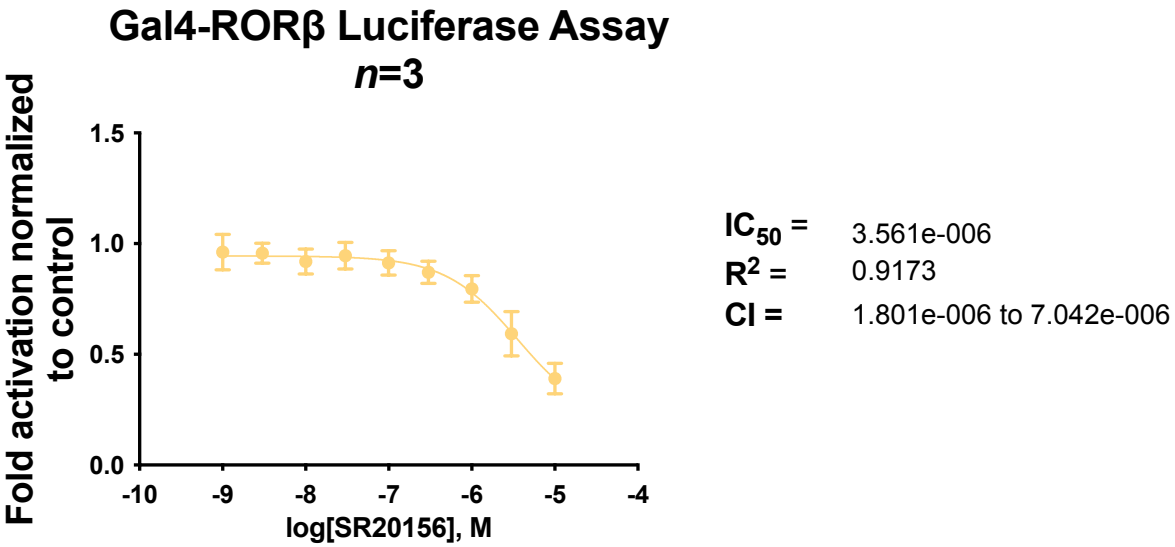

Figure 8. ***Concentration-response curve of SR20156 in the Gal4-RORβ luciferase reporter gene assay.*** HEK293 cells were transiently transfected with plasmids encoding RORβ-Gal4, a UAS-containing luciferase reporter, and eGFP as internal control using the calcium phosphate method. Cells were then treated with increasing concentrations of SR20156 for 18 h. Luminescence signals were normalized to the corresponding fluorescence signals and subsequently to the solvent control. Data are expressed as FA relative to the solvent control and are shown as mean ± SD of three biological replicates measured in technical quadruplicates. Nonlinear regression analysis resulted in an apparent IC_{50} value of 3.56 µM with an R^2 value of 0.9173. Nonlinear regression was performed using GraphPad Prism.

4.2 Comparison of SD2 and SD5

Epicorosolic acid (SD5) was identified as a hit during the initial RORβ screening and was selected for follow-up analysis. Since Corosolic acid (SD2), its corresponding C2 epimer, had previously shown inverse agonistic activity on RORγ in an earlier in-house screening project, and has also been reported in the literature as an antagonist of human RORγt [49], both compounds were investigated in parallel. The comparison was conducted to determine whether their close structural relationship translated into similar effects on RORβ- and RORγ-dependent transactivation activity.

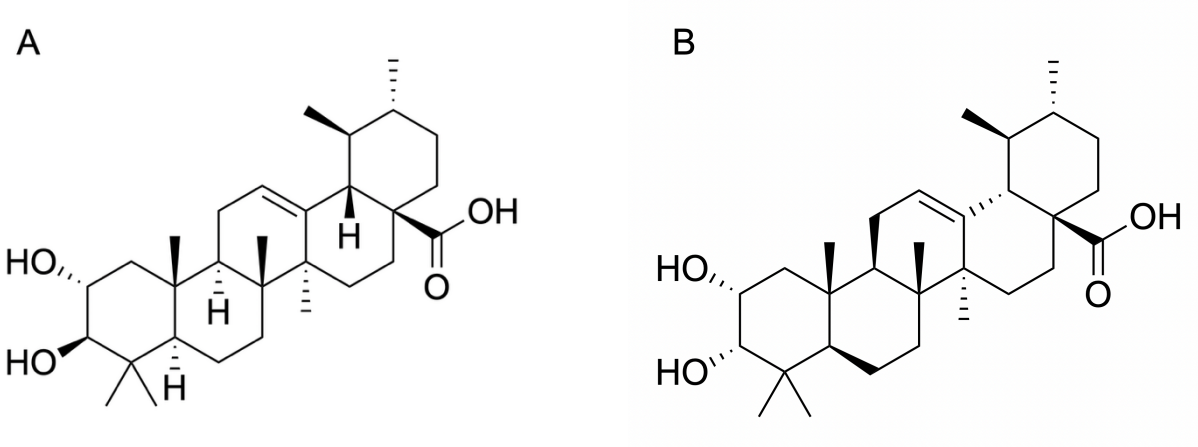

Figure 9. **Chemical structures of corosolic acid and epicorosolic acid.** Corosolic acid (A) and its C2 epimer epicorosolic acid (B) are structurally closely related triterpenoid acids that differ in the stereochemical configuration at C2. (Created with ChemDraw.)

4.2.1 Luciferase Assay Results

As shown in Figure 10, SD5 and SD2 were investigated in full-length RORβ, Gal4-RORβ, and full-length-RORγ luciferase reporter assays. In the full-length RORβ assay, SD5 reduced transactivation activity in a concentration-dependent manner, with the strongest reduction observed at 30 µM (Fig. 10a). At this concentration, SD5 reached an I_{max} of 62%, corresponding to an FA value of 0.38. Nonlinear regression analysis resulted in an IC_{50} value of 27.58 µM (Fig. 10b). However, the upper 95% confidence limit could not be determined. In contrast, SD2 did not reduce full-length RORβ-dependent transactivation activity under the tested conditions (Fig. 10a). At 30 µM, SD2 showed only a minimal reduction, with an I_{max} of 3% and an FA value of 0.97. In the Gal4-RORβ reporter assay, SD5 also reduced transactivation activity in a concentration-dependent manner, resulting in an IC_{50} value of 3.47 µM, with a broad 95% confidence interval of 0.19-64.84 µM

(Fig. 10c, d). At 30 µM, SD5 reached an I_{max} of 34%, corresponding to an FA value of 0.66.SD2 again showed no relevant reduction of the transactivation activity (Fig. 10c). The I_{max} of SD2 in this assay was 15%, corresponding to an FA value of 0.85 at 30 µM. In the full-length-RORγ assay, both SD5 and SD2 reduced transactivation activity in a concentration-dependent manner (Fig. 10e). To allow direct comparison of both compounds, concentration-response curves for SD5 and SD2 are depicted in the same graph (Fig. 10f). SD5 achieved a greater maximal reduction in transactivation activity across the tested concentration range than SD2, with the strongest reduction observed at 30 µM (FA= 0.25), corresponding to an I_{max} of 75% **(**Fig. 10e). SD2 showed a weaker maximal reduction at 30 µM, with an FA value of 0.60 and an I_{max} of 40%. Nonlinear regression analysis resulted in IC_{50} values of 7.57 µM for SD5 and 9.27 µM for SD2(Fig. 10f). In an additional UAS-Luc (Fig.11)**,** which contained the UAS-driven luciferase reporter plasmid and eGFP as internal control but no Gal4-RORβ expression plasmid**,** neither SD5 nor SD2 markedly affected the luciferase reporter signal at the tested concentrations, indicating no relevant effect on the baseline luciferase transactivation activity under these conditions.

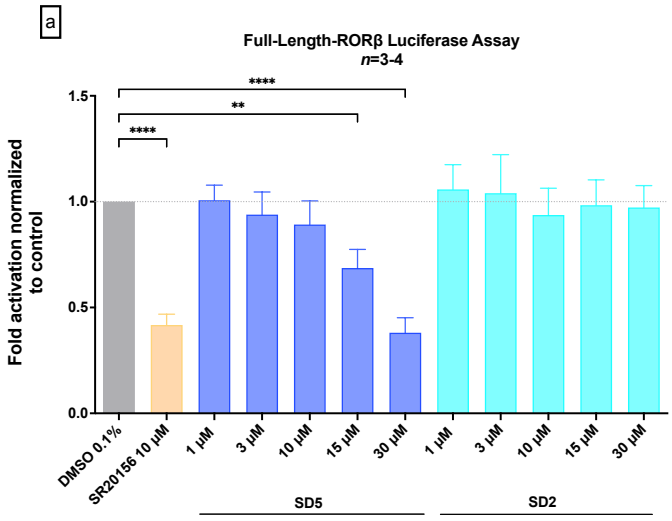
a
Full-Length-RORβ Luciferase Assay
n=3-4
Fold activation normalized to control
1.5
1.0
0.5
0.0
****
**
****
DMSO 0.1%
SR20156 10 µM
1 µM
3 µM
10 µM
15 µM
30 µM
1 µM
3 µM
10 µM
15 µM
30 µM
SD5
SD2

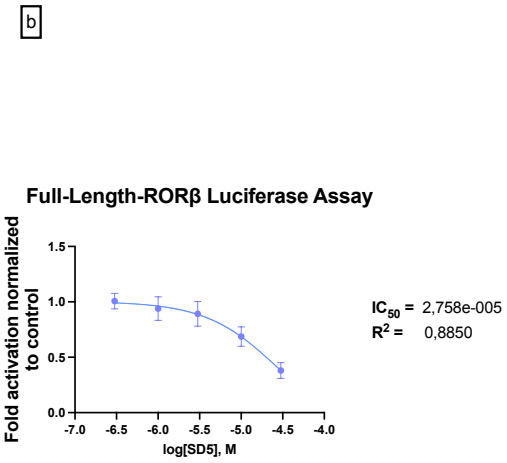
b
Full-Length-RORβ Luciferase Assay
Fold activation normalized to control
1.5
1.0
0.5
0.0
-7.0
-6.5
-6.0
-5.5
-5.0
-4.5
-4.0
log[SD5], M
IC50 = 2,758e-005
R2 = 0,8850

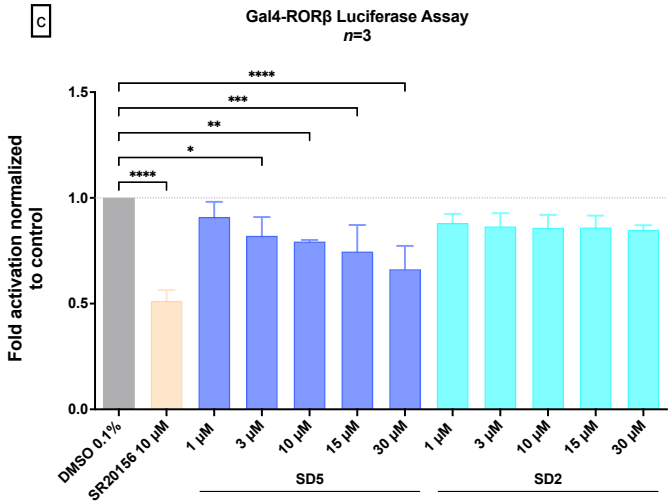
c
Gal4-RORβ Luciferase Assay
n=3
Fold activation normalized to control
1.5
1.0
0.5
0.0
****
***
**
*
****
DMSO 0.1%
SR20156 10 µM
1 µM
3 µM
10 µM
15 µM
30 µM
1 µM
3 µM
10 µM
15 µM
30 µM
SD5
SD2

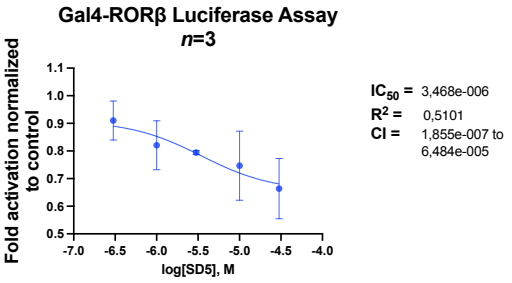
d
Gal4-RORβ Luciferase Assay
n=3
Fold activation normalized to control
1.1
1.0
0.9
0.8
0.7
0.6
0.5
-7.0
-6.5
-6.0
-5.5
-5.0
-4.5
-4.0
log[SD5], M
IC50 = 3,468e-006
R2 = 0,5101
CI = 1,855e-007 to 6,484e-005

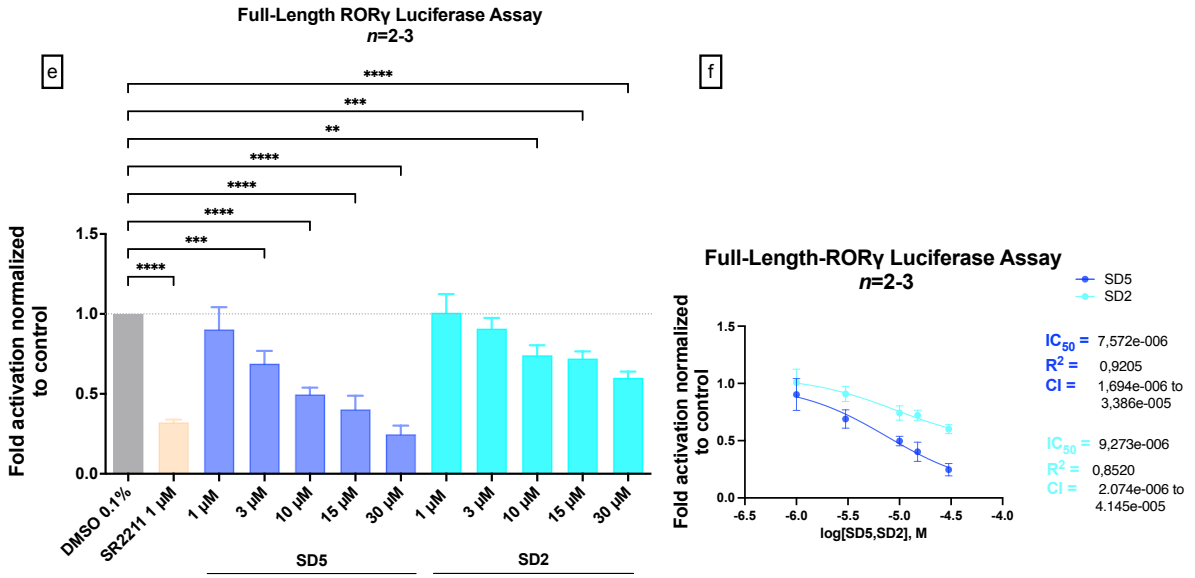

Figure 10. **Luciferase assay results for SD5 and SD2.** HEK293 cells were transiently transfected with the respective ROR reporter system and eGFP as internal control using the calcium phosphate method. Cells were then treated with increasing concentrations of SD5 or SD2 for 18 h. (A) Full-length RORβ luciferase reporter assay. SR20156 (10 µM) was used as reference inverse agonist. (B) Gal4-RORβ luciferase reporter assay. SR20156 (10 µM) was used as reference inverse agonist. (C) Full-length-RORγ luciferase reporter assay. SR2211 (1 µM) was used as reference inverse agonist. Luminescence signals were normalized to the corresponding fluorescence signals and subsequently to the solvent control DMSO 0.1%. Values are shown as FA relative to the solvent control and represent mean ± SD of two to four biological replicates measured in technical quadruplicates, as indicated in the respective panels. Statistical analysis was performed using one-way ANOVA followed by Dunnett's post hoc test. ****p ≤ 0.0001, ***p ≤ 0.001, **p ≤ 0.01, *p ≤ 0.05. Absence of significance indication denotes no statistically significant difference compared with the solvent control DMSO 0.1%. Concentration-response curves were generated for SD5 and SD2 using nonlinear regression analysis. Nonlinear regression analysis resulted in apparent IC_{50} values of 27.58 µM with an R^2 value of 0.8850 in the full-length RORβ assay, 3.47 µM with an R^2 value of 0.5101 in the Gal4-RORβ assay, and 7.57 µM with an R^2 value of 0.9552 in the full-length-RORγ assay. Nonlinear regression was performed using GraphPad Prism.

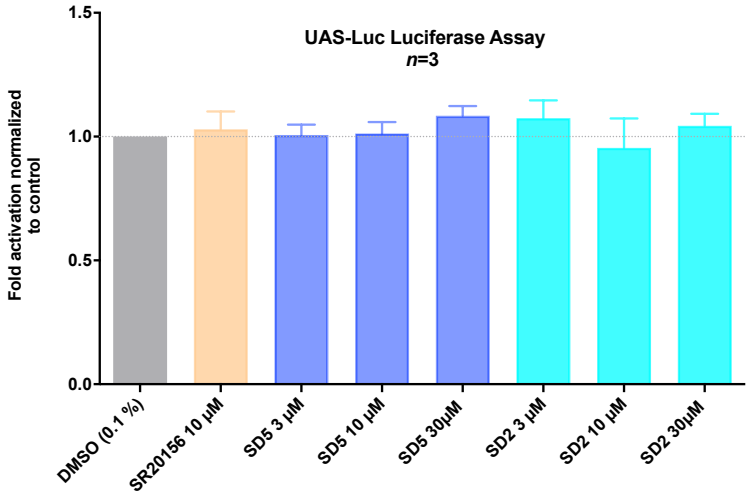

Figure 11. **Reporter control assay results for SD5 and SD2.** HEK293 cells were transiently transfected with the UAS-driven luciferase reporter plasmid and eGFP as internal control using the calcium phosphate method, without co-transfection of the Gal4-RORβ expression plasmid. Cells were then treated with SD5 or SD2 for 18 h. Luminescence signals were normalized to the corresponding fluorescence signals and subsequently to the solvent control DMSO 0.1%. Values are shown as fold activation relative to the solvent control and represent mean ± SD of three biological replicates measured in technical quadruplicates. Statistical analysis was performed using one-way ANOVA followed by Dunnett's post hoc test. ****p ≤ 0.0001, ***p ≤ 0.001, **p ≤ 0.01, *p ≤ 0.05. Absence of significance indication denotes no statistically significant difference compared with the solvent control DMSO 0.1%.

4.2.2 Resazurin Assay Results

To assess whether the effects observed in the reporter assays were associated with reduced cell metabolic activity, SD5 and SD2 were evaluated in a resazurin conversion assay in HEK293 cells. Treatment with SD5 or SD2 at concentrations ranging from 1 to 30 µM did not reduce resazurin conversion below the predefined threshold of 75 % relative to the solvent control at any tested concentration. In contrast, the cytotoxic control digitonin [46] markedly reduced the signal to 7.15 % compared to the solvent control, as confirmed by one-way ANOVA followed by Dunnett's post hoc test.

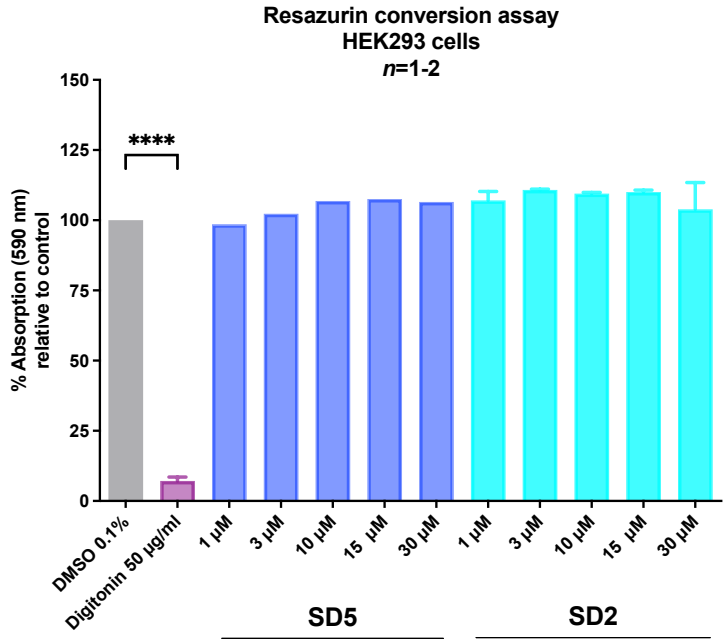

Figure 12. **Resazurin conversion assay results for SD5 and SD2.** HEK293 cells were treated with increasing concentrations of SD5 or SD2. Digitonin (50 µg/ml) was used as cytotoxic control. Resazurin conversion was determined by measuring absorbance at 590 nm and normalized to the solvent control DMSO 0.1%. Data are expressed as percentage absorption relative to the solvent control. Data are shown as mean ± SD of one to two biological replicates. Statistical analysis was performed using one-way ANOVA followed by Dunnett's post hoc test. ****p ≤ 0.0001, **p ≤ 0.01, *p ≤ 0.05. Absence of significance indication denotes no statistically significant difference compared with the solvent control DMSO 0.1%.

4.3 Phytoecdysteroid CR27

CR27 represents an inseparable mixture of regioisomeric phytoecdysteroid derivatives (Fig. 13) and was identified during the initial Gal4-RORβ screening of phytoecdysteroid-related compounds (Fig.14). Since CR27 showed increased transactivation activity compared to the solvent control and induced one of the strongest responses among the tested compounds, it was selected for further characterization in full-length RORβ and additional Gal4-based ROR reporter assays.

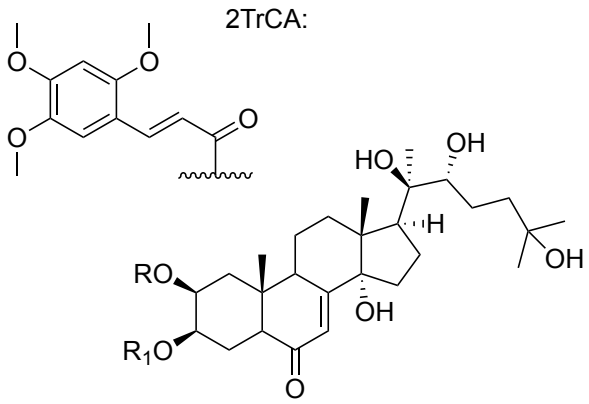

Isomer ratio by ^{1}H NMR	
C2-ester (R)	*C3-ester (R^1)*
88%	*12%*

Figure 13. **Chemical structure of CR27.** CR27 represents an inseparable mixture of regioisomeric phytoecdysteroid derivatives. The mixture consists predominantly of the C-2 ester regioisomer (R, 88%) and a smaller proportion of the C-3 ester regioisomer (R^1, 12%). (Created with ChemDraw)

4.3.1 Luciferase Assay Results

CR27 was further investigated in full-length ROR and Gal4-based luciferase assays. Due to limited compound availability, the maximum tested concentration differed between assay formats. Concentrations up to 100 µM were tested in the RORβ assays, whereas the additional receptor selectivity assays were performed up to 70 µM. In the full-length RORβ assay, CR27 increased transactivation activity, with the strongest effect observed at 100 µM. At this concentration, CR27 reached an E_{max} of 17.83 FA (Fig. 15a) Although nonlinear regression analysis resulted in an R^2 value of 0.8535, no reliable EC_{50} value could be determined (Fig. 15b). In the Gal4-RORβ assay, CR27 also increased transactivation activity at all tested concentrations, with the highest fold activation observed at 100 µM. The corresponding E_{max} was 1.89 FA (Fig. 15c). However, the response did not follow a clearly defined concentration-dependent pattern, and

nonlinear regression analysis resulted in unstable fitted parameters; therefore, no reliable EC_{50} value could be determined.

To assess whether this effect was specific for RORβ, CR27 was additionally tested in Gal4-RORα, Gal4-RORγ, and full-length-RORγ reporter assays. In the Gal4-RORα assay, CR27 increased transactivation activity in a concentration-dependent manner (Fig. 15d), resulting in an estimated EC_{50} value of 52.34 µM with an R^2 value of 0.6981 (Fig.15e). The E_{max} in this assay was 2.37 FA at 70 µM. In the Gal4-RORγ assay, CR27 showed a similar increase in transactivation activity, with an E_{max} of 1.62 FA at 70 µM and an estimated EC_{50} value of 54.05 µM (Fig. 15g). The estimated EC_{50} value was not considered reliable due to the poor fit of the nonlinear regression model (R^2= 0.3397) and the broad confidence interval of the fitted parameter. In the full-length-RORγ assay, CR27 increased transactivation activity in a concentration-dependent manner (Fig. 15h), resulting in an EC_{50} value of 16.31 µM (Fig. 15i). The E_{max} in this assay was 1.47 FA at 70 µM.

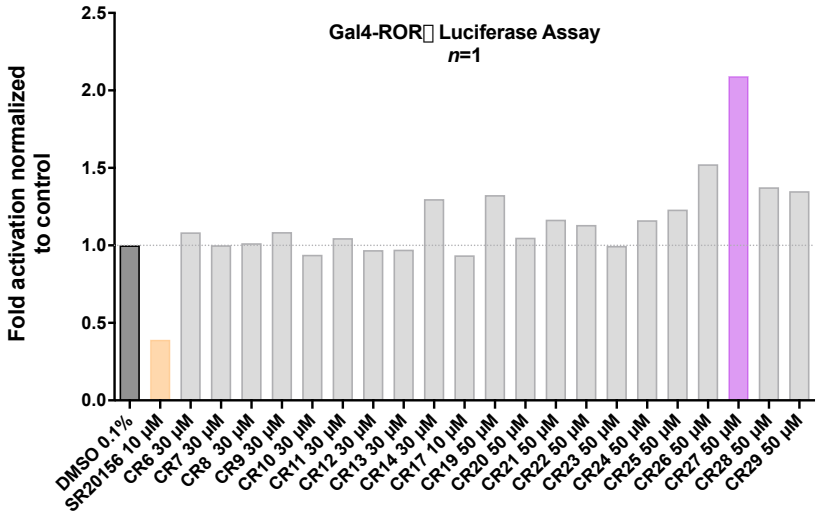

Figure 14. **Initial screening of phytoecdysteroid-related compounds in the Gal4-RORβ luciferase reporter assay.** HEK293 cells were transiently transfected with the Gal4-RORβ reporter system and eGFP as internal control using the calcium phosphate method. Cells were then treated with the indicated compounds for 18 h. SR20156 (10 µM) was used as reference inverse agonist. Luminescence signals were normalized to the corresponding fluorescence signals and subsequently to the solvent control DMSO 0.1%. Values are shown as fold activation relative to the solvent control. CR27 showed increased reporter activity compared with the solvent control and was therefore selected for further characterization.

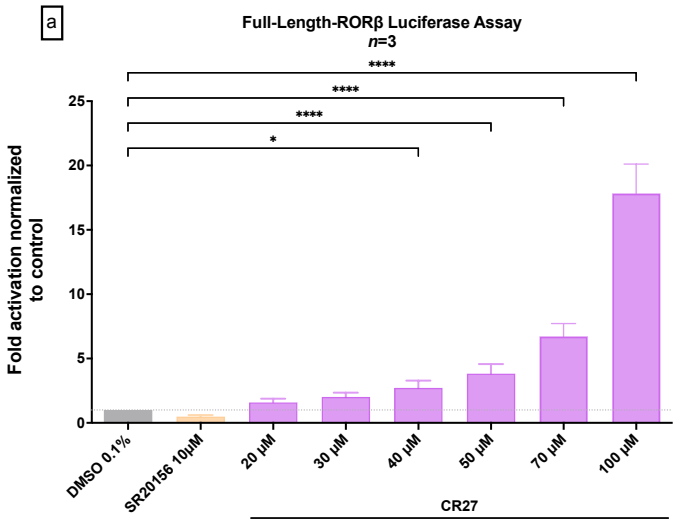
a
Full-Length-RORβ Luciferase Assay
n=3
Fold activation normalized to control
DMSO 0.1%
SR20156 10µM
20 µM
30 µM
40 µM
50 µM
70 µM
100 µM
CR27

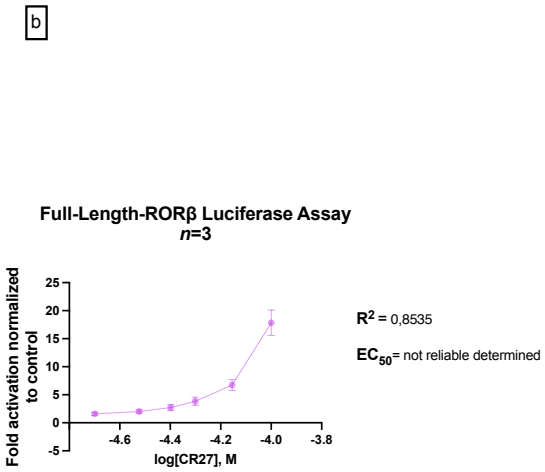
b
Full-Length-RORβ Luciferase Assay
n=3
Fold activation normalized to control
log[CR27], M
R2 = 0,8535
EC50= not reliable determined

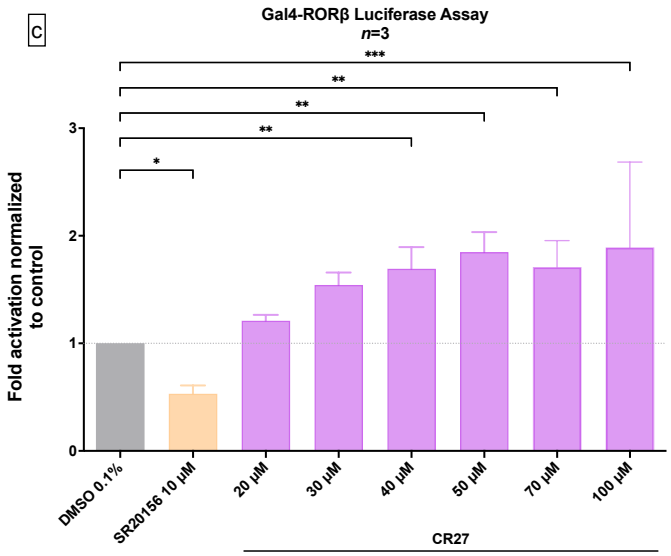
c
Gal4-RORβ Luciferase Assay
n=3
Fold activation normalized to control
DMSO 0.1%
SR20156 10 µM
20 µM
30 µM
40 µM
50 µM
70 µM
100 µM
CR27

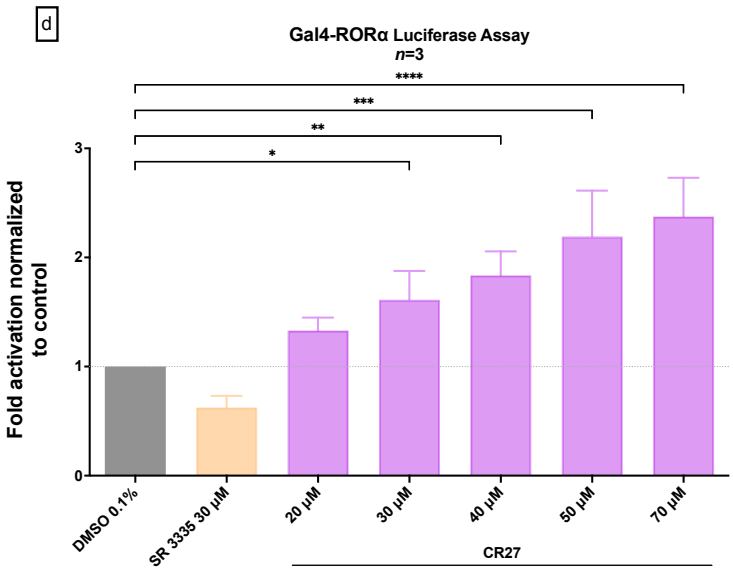
d
Gal4-RORα Luciferase Assay
n=3
Fold activation normalized to control
DMSO 0.1%
SR 3335 30 µM
20 µM
30 µM
40 µM
50 µM
70 µM
CR27

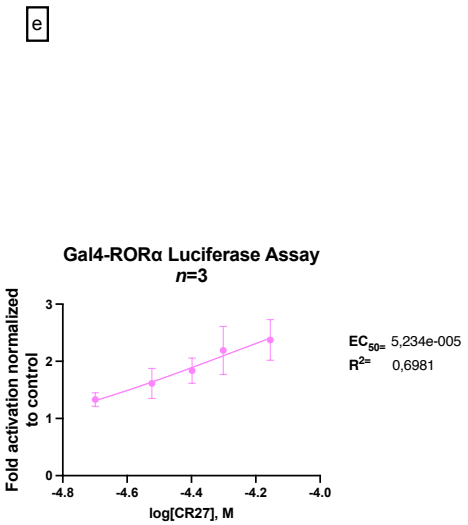
e
Gal4-RORα Luciferase Assay
n=3
Fold activation normalized to control
log[CR27], M
EC50= 5,234e-005
R2= 0,6981

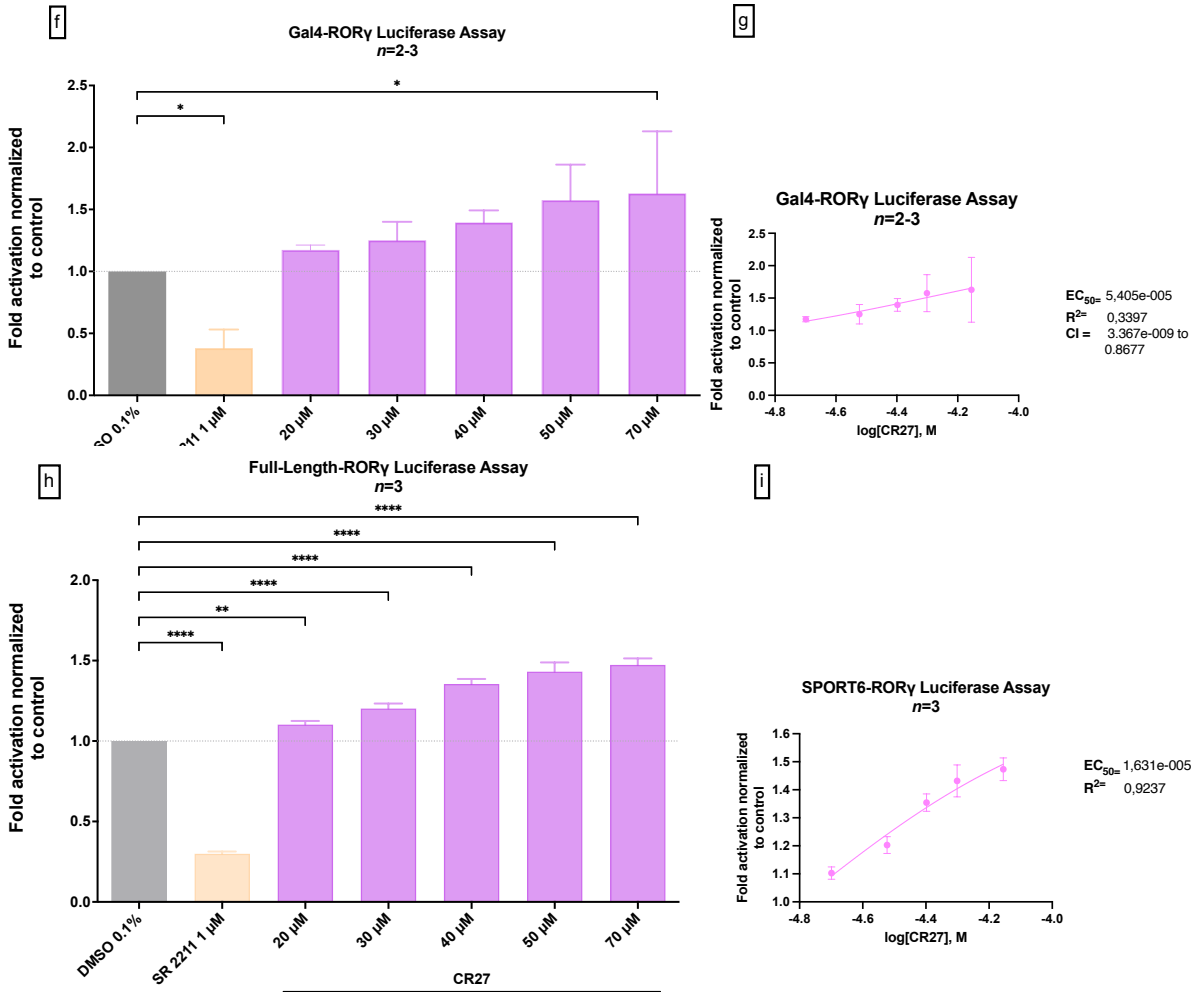

Figure 15. **Luciferase assay results for CR27.** HEK293 cells were transiently transfected with the respective ROR reporter system and eGFP as internal control using the calcium phosphate method. Cells were then treated with increasing concentrations of CR27 for 18 h. (A) Full-length RORβ luciferase reporter assay. SR20156 (10 µM) was used as reference inverse agonist. (B) Gal4-RORβ luciferase reporter assay. SR20156 (10 µM) was used as reference inverse agonist. (C) Gal4-RORα luciferase reporter assay. SR3335 (30 µM) was used as reference inverse agonist. (D) Gal4-RORγ luciferase reporter assay. SR2211 (1 µM) was used as reference inverse agonist. E) Full-length-RORγ luciferase reporter assay. SR2211 (1 µM) was used as reference inverse agonist. Luminescence signals were normalized to the corresponding fluorescence signals and subsequently to the solvent control DMSO 0.1%. Values are shown as FA relative to the solvent control and represent mean ± SD of two to three biological replicates measured in technical quadruplicates, as indicated in the respective panels. Statistical analysis was performed using one-way ANOVA followed by Dunnett's post hoc test. ****p ≤ 0.0001, ***p ≤ 0.001, **p ≤ 0.01, *p ≤ 0.05. Absence of significance indication denotes no statistically significant difference compared with the solvent control DMSO 0.1%. Concentration-response curves were generated using nonlinear regression analysis. In the full-length RORβ assay, no reliable EC_{50} value could be determined. In the Gal4-RORα assay, nonlinear regression analysis resulted in an EC_{50} value of 52.34 µM. In the Gal4-RORγ assay, nonlinear regression analysis resulted in an EC_{50} value of 54.05 µM; however, this estimate was not considered reliable due to the low goodness of fit and broad confidence interval. In the Full-length-RORγ assay, nonlinear regression analysis resulted in an EC_{50} value of 16.31 µM. Nonlinear regression was performed using GraphPad Prism.

To further assess whether the CR27-induced increase in transactivation activity was receptor-dependent, CR27 was tested in additional reporter control assays without Gal4-RORβ or full-length RORβ (Fig. 16). In these assays, HEK293 cells were transfected with the respective luciferase reporter plasmid and eGFP as internal control, but without the corresponding RORβ expression plasmid. In the RORE-Luc assay, CR27 increased the reporter signal to 8.54-fold activation at 100 µM, whereas the corresponding increase in the full-length RORβ assay was 17.83-fold activation. Thus, the increase observed in the RORE-Luc assay was lower than the response obtained in the full-length RORβ assay. In the UAS-Luc assay, CR27 increased the reporter signal to 2.16-fold activation at 100 µM, compared with 1.89-fold activation in the Gal4-RORβ assay. CR27 therefore increased transactivation activity in both control assays in a concentration-dependent manner

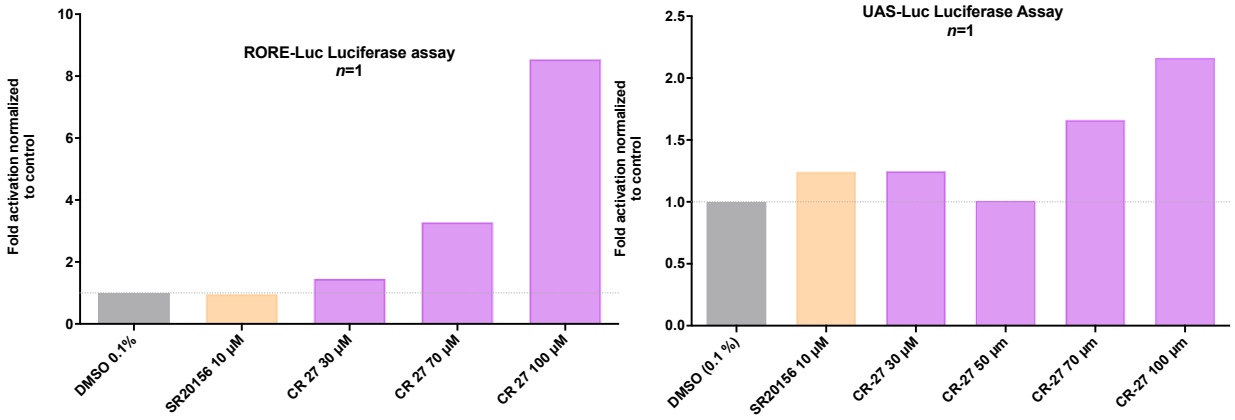

Figure 16. **Reporter control assay results for CR27.** HEK293 cells were transiently transfected with the respective luciferase reporter plasmid and eGFP as internal control using the calcium phosphate method. Cells were then treated with increasing concentrations of CR27 for 18 h.(A) RORE-Luc reporter assay. (B) UAS-Luc reporter assay. Luminescence signals were normalized to the corresponding fluorescence signals and subsequently to the solvent control DMSO 0.1%.

4.3.2 Results for Resazurin Assay

To assess whether the effects observed in the reporter assays were associated with reduced cell metabolic activity, CR27 was evaluated in a resazurin conversion assay in HEK293 cells (Fig. 17). Treatment with CR27 at concentrations ranging from 20 to 100 µM did not reduce resazurin conversion below the predefined threshold of 75 % relative to the solvent control at any tested concentration. In contrast, the cytotoxic control digitonin [46] markedly reduced the signal to 7.23 % of the solvent control.

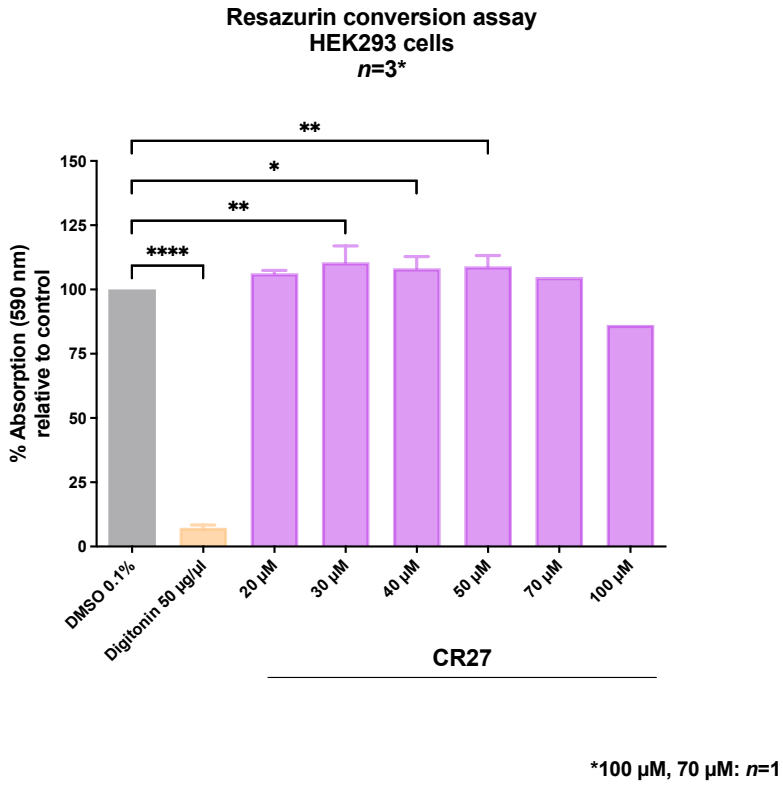

Figure 17. **Resazurin conversion assay results for CR27.** HEK293 cells were treated with increasing concentrations of CR27. Digitonin (50 µg/ml) was used as cytotoxic control. Resazurin conversion was determined by measuring absorbance at 590 nm and normalized to the solvent control DMSO 0.1%. Data are expressed as percentage absorption relative to the solvent control and are shown as mean ± SD of three biological replicates, except for CR27 100 µM and 70 µM, which were measured once and are therefore shown without SD. Statistical analysis was performed using one-way ANOVA followed by Dunnett's post hoc test. ****p ≤ 0.0001, **p ≤ 0.01, *p ≤ 0.05. Absence of significance indication denotes no statistically significant difference compared with the solvent control DMSO 0.1%.

5 Discussion

5.1 SR20156 supports the use of the Gal4-RORβ assay for screening RORβ modulators

Before screening potential RORβ modulators, it was necessary to identify a suitable reference compound and confirm that the Gal4-RORβ luciferase reporter assay responded reliably under the experimental conditions used in this thesis. SR20156 was selected as reference inverse agonist and positive control, since ATRA, although described as a ligand of RORβ [20], is limited by its light sensitivity and instability under non-protected conditions [28].

SR20156 reduced Gal4-RORβ transactivation activity in a concentration-dependent manner, confirming that the established assay was suitable for detecting changes in RORβ activity. Nonlinear regression analysis resulted in an IC_{50} value of 3.56 µM. This value was higher than the IC_{50} reported for SR20156 in the literature, where SR20156 showed potent activity at RORβ with an IC_{50} value of < 0.010 µM. Doebelin et al. also reported that SR20156 showed activity on RORγ, although to a lesser extent, with an IC_{50} value of > 3.0 µM [28] Thus, SR20156 is not fully selective for RORβ, but still provides a useful reference compound for monitoring reduced RORβ transactivation activity in the established assay. The difference between the IC_{50} value observed in this thesis and the literature value may be explained by assay-dependent factors, since reporter gene assays measure transcriptional output rather than direct ligand binding. The higher IC_{50} value observed in this thesis may therefore reflect differences between the experimental setups. Overall, the SR20156 data support the use of the established Gal4-RORβ assay for the screening of potential RORβ modulators.

5.2 SD5 and SD2 show receptor subtype-dependent effects in ROR reporter assays

SD5 and SD2 were compared in parallel in full-length RORβ, Gal4-RORβ, and full-length-RORγ reporter assays because they are structurally closely related C2 epimers. This comparison made it possible to investigate whether their small stereochemical difference resulted in different effects on RORβ- and RORγ-mediated transactivation activity.

In the full-length RORβ reporter assay, SD5 reduced transactivation activity mainly at higher concentrations, whereas SD2 did not show a comparable effect. This indicates that the structural difference between SD5 and SD2 may contribute to their different effects on RORβ transactivation activity. However, the IC_{50} value of 27.58 µM for SD5 should be interpreted with caution, since the upper 95% confidence limit could not be determined and the value was close to the upper end of the tested concentration range. This was likely due to the concentration-response curve not reaching a clearly defined lower plateau within the tested concentration range. Thus, the data support a concentration-dependent effect of SD5 in the full-length RORβ assay, although the potency estimate remains uncertain under the tested conditions.

In the Gal4-RORβ reporter assay, SD5 also reduced transactivation activity in a concentration-dependent manner, whereas SD2 again did not show a relevant effect. Therefore, the difference between SD5 and SD2 observed in the full-length RORβ assay was also present in the Gal4-RORβ system. For SD5, the IC_{50} value was lower in the Gal4-RORβ assay than in the full-length RORβ assay, with values of 3.47 µM and 27.58 µM, respectively. However, the relatively broad confidence interval of 0.19-64.84 µM indicates that this potency estimate should still be interpreted with caution. The different apparent potencies observed in the full-length and Gal4-RORβ assays may reflect differences between the assay formats, since the Gal4-based system uses the ligand-binding domain fused to the Gal4 DBD, whereas the full-length assay contains the complete receptor. The UAS-Luc control assay showed that SD5 and SD2 did not markedly affect the UAS-Luc reporter signal, suggesting no relevant unspecific effect on the UAS-driven reporter system. However, a corresponding RORE-Luc-only control assay would be required to exclude receptor-independent effects in the full-length ROR assays.

In contrast to the RORβ assays, both SD5 and SD2 reduced RORγ-dependent transactivation activity in the full-length-RORγ assay. At 30 µM, SD5 reduced transactivation activity to an FA value of 0.25**,** whereas SD2 reduced transactivation activity to an FA value of 0.60, indicating a stronger maximal reduction by SD5. The apparent IC_{50} values were in a similar range, with 7.57 µM for SD5 and 9.27 µM for SD2**.**This suggests that the stereochemical difference between SD5 and SD2 may be more relevant for RORβ than for RORγ under the tested conditions. Nevertheless, the

results should be interpreted as effects on transactivation activity and not as direct evidence for receptor binding.

Taken together, SD5 showed concentration-dependent effects in both RORβ assay formats and in the full-length-RORγ assay, whereas SD2 did not show relevant activity on RORβ but reduced RORγ-dependent transactivation activity. These findings suggest receptor subtype-dependent differences between the two C2 epimers. The apparent selectivity of SD2 toward RORγ is particularly interesting, as comparison with SD5 may provide a useful starting point for structure-activity relationship studies. Such studies could help identify structural features that determine receptor subtype preference and may support the development of more selective compounds for RORβ in the future. The resazurin conversion assay showed that none of the compounds reduced cell metabolic activity below the predefined threshold at the tested concentrations, implying that the observed reporter assay effects were not caused by reduced metabolic activity. However, further experiments would be required to confirm whether these effects result from direct receptor modulation. Potential follow-up experiments could include direct binding assays, target gene expression analysis and additional receptor selectivity assays.

5.3 CR27 increases luciferase reporter signals across multiple assay formats

While SD5 and SD2 were investigated mainly for their ability to reduce ROR transactivation activity, CR27 produced an activation-like increase in the luciferase reporter signal. Although inhibition of RORβ may be of interest in the context of bone-related diseases, compounds that increase RORβ-associated reporter signals can still be useful tools for investigating RORβ biology. Therefore, CR27 was selected for further investigation after showing increased transactivation activity during the initial Gal4-RORβ screening of phytoecdysteroid-related compounds.

In the full-length RORβ reporter assay, CR27 strongly increased transactivation activity, with the highest effect observed at 100 µM. Although nonlinear regression analysis resulted in an R^2 value of 0.8535, no reliable EC_{50} value could be determined. This was likely due to unstable fitted parameters and the absence of a clearly defined

concentration-response relationship over the tested concentration range. The strong increase in this assay initially suggested a possible agonistic effect on RORβ.

In the Gal4-RORβ assay, CR27 also increased transactivation activity at all tested concentrations. However, the response did not follow a clear concentration-dependent pattern, and nonlinear regression resulted in biologically implausible fitted parameters. Therefore, no reliable EC_{50} value could be assigned for CR27 in the Gal4-RORβ assay.

To assess whether the observed effect was specific for RORβ, CR27 was further tested in Gal4-RORα, Gal4-RORγ, and full-length-RORγ reporter assays. CR27 increased transactivation activity in all three assays, although the reliability of the calculated EC_{50} values differed between assay formats. In the Gal4-RORα assay, an estimated EC_{50} value of 52.34 µM was obtained, but the confidence interval could not be determined, indicating that this value should be interpreted with caution. In the Gal4-RORγ assay, the estimated EC_{50} value was 54.05 µM, but the low R^2 value and very broad confidence interval indicated that the fit was not reliable. In contrast, the full-length-RORγ assay showed a clearer concentration-dependent increase in transactivation activity, resulting in an EC_{50} value of 16.31 µM with an R^2 value of 0.9237.

Taken together, CR27 increased transactivation activity in several ROR reporter assays rather than showing a selective effect on RORβ. Additional reporter control assays showed that CR27 also increased activity in the RORE-Luc and UAS-Luc systems in the absence of Gal4-RORβ or full-length RORβ. This supports the interpretation that the activity observed in the Gal4-based assays may arise, at least in part, from interference with the reporter system. However, the increase in the RORE-Luc control assay was lower than the response observed in the full-length RORβ assay at 100 µM CR27, with FA values of 8.54 and 17.83, respectively. Therefore, reporter-associated effects may not fully explain the strong increase seen in the full-length RORβ system, and a possible RORβ-related component cannot be excluded. Nevertheless, the broad activity across several reporter systems indicates that the CR27 data should be interpreted as changes in transactivation activity and not as direct evidence for receptor binding or selective receptor modulation.

The resazurin conversion assay showed that CR27 did not reduce cell metabolic activity below the predefined threshold at the tested concentrations. Reduced metabolic activity

would be more likely to mimic inhibitory effects than to explain the observed increase in transactivation activity. Therefore, the main limitation of the CR27 data remains the possible reporter-associated effect. Further experiments, including direct binding assays, additional receptor selectivity assays, and target gene expression analysis, would be required to clarify whether CR27 directly modulates ROR receptors.

6 Conclusion

In conclusion, this thesis confirmed that the Gal4-RORβ luciferase reporter gene assay was suitable for the screening of potential RORβ modulators. SR20156 confirmed the responsiveness of the assay and was used as a positive control for further experiments. Screening of natural products and derivatives identified SD5 and CR27 as compounds that showed activity in RORβ luciferase reporter assays, whereas SD2 showed no relevant activity on RORβ under the tested conditions. SD5 reduced RORβ-mediated transcriptional activity in both full-length RORβ and Gal4-RORβ assays, while CR27 increased the luciferase reporter assay readout but showed possible reporter-associated effects, limiting the interpretation of its receptor-specific activity.

The comparison of SD5 and SD2 suggests that small stereochemical differences between structurally related compounds may influence their effects in ROR reporter assays. Since RORβ has been associated with bone-related processes, including osteoblast biology, the identification of compounds affecting RORβ activity may be relevant for future studies in the context of bone metabolism and osteoporosis. However, the results obtained in this thesis are based on reporter gene assays and therefore require further validation. Further experiments will be needed to clarify whether the observed effects reflect direct modulation of RORβ.

7 Declaration of AI in the writing process

ChatGPT, Perplexity and DeepL were used to support linguistic revision of this thesis. All generated suggestions were reviewed and adapted by the author, who remains fully responsible for the final content.

8 Appendix

Table 11. **Activities of compounds tested on Gal4-ROR*β***

Luciferase Assay Gal4-RORβ			
Label	**Name**	**Fold Activation against DMSO**	**Tested concentration**
447		0,94	10 µg/ml
448		0,99	10 µg/ml
449		0,95	10 µg/ml
450		0,87	10 µg/ml
452		0,88	10 µg/ml
453		1,42	10 µg/ml
454		0,98	10 µg/ml
455		0,94	10 µg/ml
456		0,81	10 µg/ml
459		0,87	10 µg/ml
460		1,07	10 µg/ml
461		1,04	10 µg/ml
462		0,98	10 µg/ml
463		0,88	10 µg/ml
464		0,95	10 µg/ml
465		0,90	10 µg/ml
466		0,95	10 µg/ml
467		0,90	10 µg/ml
468		0,93	10 µg/ml
471		0,92	10 µg/ml
472		0,93	10 µg/ml
475		0,98	10 µg/ml
477		0,94	10 µg/ml
478		0,78	10 µg/ml
479		0,91	10 µg/ml
480		0,72	10 µg/ml
481		0,77	10 µg/ml
482		0,93	10 µg/ml
483		0,86	10 µg/ml

484	1,00	10 µg/ml
485	0,90	10 µg/ml
486	0,91	10 µg/ml
487	0,89	10 µg/ml
488	0,91	10 µg/ml
489	0,66	10 µg/ml
490	0,65	10 µg/ml
491	0,69	10 µg/ml
492	0,78	10 µg/ml
493	1,06	10 µg/ml
494	0,75	10 µg/ml
640	1,04	10µM
641	0,89	10µM
700	1,03	10µM
701	0,98	10µM
702	1,00	10µM
704	1,15	10µM
705	1,19	10µM
707	1,32	10µM
711	1,08	10µM
712	0,95	10µM
727	0,91	10µM
728	0,88	10µM
729	1,14	10µM
739	1,11	10µM
757	1,10	10µM
759	1,31	10µM
761	1,27	10µM
766	1,01	10µM
767	0,77	10µM
770	1,14	10µM
773	0,74	10µM
774	0,87	10µM
776	0,73	10µM
777	0,85	10µM
778	1,02	10µM
779	0,89	10µM
780	1,12	10µM
782	1,21	10µM
783	0,77	10µM
801	0,82	10µM
802	0,93	10µM
803	0,77	10µM
804	0,97	10µM
806	1,02	10µM
807	0,65	10µM
808	1,26	10µM

1101		0,95	10μM
1102		0,86	10μM
1103		1,08	10μM
1228		0,90	10μM
1229		0,84	10μM
1230		0,78	10μM
1231		0,87	10μM
1232		0,82	10μM
1233		0,88	10μM
1234		0,84	10μM
1240		0,02	10μM
1241		0,03	10μM
1242		0,07	10μM
2765		0,13	10μM
BP-1	Broussoflavonol A	0,65	10 μM
BP-2	Broussoflavonol B	0,35	10 μM
BP-3	Broussoflavonol I	0,30	10 μM
BP-4	Diprenylflavon	0,46	10 μM
BP-5	Geranylflavon	0,78	10 μM
BP-6	Isoliquiritigenin	1,76	10 μM
BP-7	Kazinol A	0,94	10 μM
BP-8	Kazinol B	0,95	10 μM
BP-9	Kazinol J	0,81	10 μM
BP-10	Kazinol M	0,34	10 μM
BP-11	Kazinol U	0,88	10 μM
BP-12	3'-prenyl-3',4',7-trihydroxyflavan	1,42	10 μM
BP-13	5,7-dihydroxychromone	0,62	10 μM
BP-14	Umbelliferone	0,84	10 μM
BP-15	Marmesin	1,52	10 μM
BP-16	Rutaretin	1,09	10 μM
BP-17	8-methoxymarmesin	1,06	10 μM
BP-18	8-hydroxyxanthyletin	1,14	10 μM
BP-19	Fipsomin	0,84	10 μM
BP-20	Fipsotwin	1,09	10 μM
FCa-1	Psoralen	1,07	10 μM
FCa-2	Bergapten	1,06	10 μM
FCy-1	Ficusin A	0,70	10 μM
FCy-2	Ficusin B	0,62	10 μM
FCy-4	Ficusin D	1,38	10 μM
ZB-1	Ursolic acid	0,79	10 μM
ZB-2	Oleanolic acid	0,94	10 μM
ZB-3	Betulinic acid	0,99	10 μM
ZB-4	21α-hydroxyursolic acid	0,98	10 μM
ZB-5	Betulin	1,20	10 μM
ZB-6	Loliolide	0,99	10 μM
SD-1	Euscaphic acid	0,83	10 μM

SD-2	Corosolic acid	0,94	10 µM
SD-3	Maslinic acid	0,86	10 µM
SD-4	Pomolic acid	0,83	10 µM
SD-5	3-epi-corosolic acid	0,67	10 µM
AM-1	Arctigenin	0,66	10 µM
AM-2	Arctiin	0,89	10 µM
AM-3	Lappaol A	0,62	10 µM
AM-4	Isolappaol A	0,77	10 µM
AM-5	Lappaol C	1,11	10 µM
AM-6	Isolappaol C	0,96	10 µM
AM-7	Matairesinol	0,93	10 µM
AM-8	Diarctigenin		
DC_1		1,25	10 µM
DC_2		1,00	10 µM
DC_3		1,07	10 µM
DC_4		1,26	10 µM
DC_5		1,36	10 µM
DC_6		0,88	10 µM
DC_7		1,22	10 µM
SCH_10-6		0,51	10 µM
SCH_12-5		0,76	10 µM
SCH_9/A		0,65	10 µM
AF_2		1,10	10 µM
KS-01	Mesuaxanthone A	0,79	10 µM
KS-02	Osajaxanthone	1,14	
KS-03	Toxyloxanthone C	0,95	
KS-04	Macluraxanthone	1,09	10 µM
KS-05	Gerontoxanthone A	1,08	10 µM
KS-06	6-deoxyisojacareubin	0,77	10 µM
KS-07	1,3,5,6-tetrahydroxyxanthon-4-glucoside	1,08	10 µM
KS-08	Toxyloxanthone B	0,97	10 µM
KS-09	Gerontoxanthone C	0,81	10 µM
KS-11	Osajin	0,89	10 µM
KS-12	Pomiferin	0,71	10 µM
PT-01	Mimulone	0,53	10 µM
PT-02	Tomentone II	0,25	10 µM
PT-03	Diplacone	0,17	10 µM
PT-04	Diplacol	0,47	10 µM
PT-05	Tomentone B	0,55	10 µM
PT-06	3'-*O*-Methyl-5'-hydroxydiplacone	0,32	10 µM
PT-07	Tomentodiplacone	0,60	10 µM
PT-08	3'-*O*-Methyldiplacol	0,66	10 µM

PT-09	3,3',4',5,7-Pentahydroxy-6-[6-hydroxy-3,7-dimethyl-2(*E*),7-octadienyl]flavanone	0,53	10 µM
PT-10	3'-*O*-Methyl-5'-methoxydiplacone	0,66	10 µM
CB2	Cannflavin B	0,93	10 µM
ER-01	Eckol	0,90	10 µM
ER-02	Fucofuroeckol A	0,89	10 µM
ER-03	Phlorofucofuroeckol A	0,92	10 µM
ER-04	Dieckol	0,88	10 µM
ER-05	Dibenzodioxin-fucodiphloroethol	0,70	10 µM
ER-06	Phlorotannin 974-A	0,83	10 µM
FB1	Alfatradiol	0,74	10 µM
FB2	Beclomethasone dipropionate	0,91	10 µM
FB3	Dienestrol	0,89	10 µM
FB4	Diethylstilbestrol	0,82	10 µM
FB5	Digitonin	1,27	10 µM
FB6	Digitoxin	0,37	10 µM
FB8	Estradiol hemihydrate	0,85	10 µM
FB9	Estradiol valerate	1,04	10 µM
FB10	Estriol	1,12	10 µM
FB11	17α-Ethynylestradiol	0,68	10 µM
FB12	Fluocinolone acetonide	0,88	10 µM
FB13	Gestoden	1,04	10 µM
FB14	Hydrocortisone acetate	1,00	10 µM
FB15	Hydrocortisone butyrate	1,10	10 µM
FB16	Mesterolone	1,20	10 µM
FB17	Methylprednisolone	1,03	10 µM
FB18	Norethisterone acetate	1,06	10 µM
FB19	Norgestimate	0,85	10 µM
FB20	Estradiol benzoate	1,10	10 µM
FB21	Prednisolone acetate	1,24	10 µM
FB22	Testosterone propionate	1,33	10 µM
FB23	Testosterone	1,07	10 µM
FB24	Triamcinolone acetonide	0,49	10 µM
FB25	All-trans retinoic acid	0,82	10 µM
FB26	JK-940		10 µM
FB27	JK-938	1,65	10 µM
FB28	JK-945	1,17	10 µM
FB29	JK-941	1,29	10 µM
FB30	MG-18H	1,60	10 µM
FB31	MG-22H	1,59	10 µM

FB32	MG-30H	1,30	10 µM
FB33	MG-33H	0,85	10 µM
FB34	MGI-39		
FB35	MiH-12	1,31	10 µM
FB36	MiH-17	1,61	10 µM
FB37	MiH-38	1,18	10 µM
FB38	MiH-52	1,29	10 µM
FB39	MiH-58	1,60	10 µM
FB40	MiH-66		
FB41	MiH-70	1,50	10 µM
FB42	MiH-76	1,21	10 µM
FB43	MiH-77		
FB44	MiH-78	1,19	10 µM
FB45	MiH-86	1,45	10 µM
FB46	Desmosterol	1,22	5 µM
FB47	SH-42	1,37	10 µM
FB48	Chenodeoxycholic acid	0,98	10 µM
FB49	Cholic acid	0,89	10 µM
FB52	Amiodarone	1,10	10 µM
FB53	IK1	0,88	10 µM
FB54	Benzbromarone	0,91	10 µM
FB55	cid5	0,76	10 µM
FB56	Orphenadrine-HCl	1,09	10 µM
FB57	Triparanol	0,38	10 µM
	Dronedarone-HCl	2,86	10 µM
FB58			
FB59	cid081	0,36	10 µM
FB60	cid091	1,18	10 µM
FB61	IK69	0,86	10 µM
FB62	IK86	0,94	10 µM
Bempedoic acid		1,18	15 µM
BMS		1,33	15 µM
NDI		0,84	10 µM
Ketokonazole		1,12	10 µM
Pitavastatin		0,81	10 µM
P-Sali	Modified salicylic acid	0,96	10 µM
Pen-Naprox	Modified naproxen	0,97	10 µM
Naproxen		0,96	10 µM
P*	P* (H2S donor)	1,27	100 µM
Bergapten		1,08	10 µM
Bordeaux R		1,20	10 µM
Catechin		1,06	10 µM
Pelargonidin chloride		1,22	10 µM
Tartrazin		1,09	10 µM
WL2		1,01	10 µM
WL4		1,10	2.5 µM

KO161		1,07	10 µM
KO167		1,42	1.25 µM
KO168		1,10	10 µM
KO113		1,00	10 µM
KO136		0,92	10 µM
ZG8		1,09	10 µM
ZG10		1,09	10 µM
KO162		1,36	1.25 µM
KO169		1,05	10 µM
KO171		1,13	10 µM
KO172		1,21	10 µM
KO176		1,05	10 µM
GSR-G167-A2-1		0,96	10 µM
GSR-G167-A2-2		1,05	10 µM
GSR-G168-A2		0,94	10 µM
GSR-G169-A2		0,94	10 µM
Abietic acid		1,32	10 µM
Berberine		1,09	10 µM
Taxifolin		0,87	10 µM
Naringenin		0,96	10 µM
Levamisole		0,91	10 µM
Fisetin		1,09	10 µM
Alkannin/Shikonin		0,65	5 µM
Quercetin		1,08	10 µM
Kaempferol			
Cephaelin		0,48	25 µM
Emetine		0,49	10 µM
Resveratrol		1,86	10 µM
Luteolin		0,86	10 µM
Esculetin		0,77	10 µM
Xanthohumol		0,65	10 µM
Urolithin A		1,09	30 µM
WS 2-4		1,01	30 µM
WS 2-11		1,18	30 µM
WS 2-12		0,01	30 µM
WS 3-5		0,98	30 µM
WS 3-7		0,99	30 µM
WS 3-15		1,06	30 µM
WS 3-16		1,51	30 µM
WS 4-3		1,08	30 µM
WS 4-5		0,59	30 µM
WS 4-6		0,09	30 µM
WS 4-8		0,77	30 µM
WS 4-10		1,01	30 µM
WS 5-16		0,01	30 µM
CR1	20-Hydroxyecdysone	1,13	30 µM

CR2	20-Hydroxyecdysone 20,22-monoacetonide	1,08	30 µM
CR3	20-Hydroxyecdysone 2,3; 20,22-diacetonide	1,02	30 µM
CR4	Ecdysone	1,06	30 µM
CR5	Calonysterone	1,10	30 µM
CR6	Calonysterone 20,22-phenylboronate	1,08	30 µM
CR7	Dacryhainansterone	1,00	30 µM
CR8	Rubrosterone	1,01	30 µM
CR9	Poststerone	1,09	30 µM
CR10	Shidasterone	0,94	30 µM
CR11	Ajugalactone	1,05	30 µM
CR12	Ajugasterone C	0,97	30 µM
CR13	BKE20	0,97	30 µM
CR14	14β-14,15-Dihydrocalonysterone (BKE15)	1,30	30 µM
CR16	20-Hydroxyecdysone 2-cinnamate (HMB 16 1B)		30 µM
CR17	FP6A	0,94	10 µM
CR18	Calonysterone 2,3; 20,22 diacetonide	11254,00	30 µM
CR19	Makisterone A	1,32	50 µM
CR20	Makisterone C	1,05	50 µM
CR21	14β-14-deoxy-20-hydroxyecdysone (BEK16)	1,17	50 µM
CR22	BEK17	1,13	50 µM
CR23	BKE19	1,00	50 µM
CR24	14β-20(S)-14-deoxy-20-hydropoststerone (BKE21)	1,16	50 µM
CR25	14β-17α-14-deoxypoststerone (BKE22)	1,23	50 µM
CR26	HME_MDCA	1,52	50 µM
CR27	HME_2TrCA	2,09	50 µM
CR28	HM_E_TriCA	1,37	50 µM
HESP	Hesperetin	1,27	10 µM
ERIO	Eriodictyol	1,04	10 µM
TAX	Taxifolin	0,92	10 µM
AMP	Ampelopsin	1,05	10 µM
NOX	Naringenin oxime	0,99	10 µM
HOX	Hesperetin oxime	0,99	10 µM
EOX	Eriodictyol oxime	0,92	10 µM
TAX3OX	Taxifolin-3-oxime	1,02	10 µM
TAX4OX	Taxifolin-4-oxime	1,05	10 µM
AMP3OX	Ampelopsin-3-oxime	0,95	10 µM

AMP4OX	Ampelopsin-4-oxime	0,96	10 µM
LOX	Liquiritigenin oxime	1,20	10 µM
GCY	Glycycoumarin	0,92	10 µM
LICA	Licochalcone A	0,51	10 µM
LICB	Licochalcone B	1,31	10 µM
LICD	Licochalcone D	0,66	10 µM
LICE	Licochalcone E	0,47	10 µM
ECH	Echinatin	1,61	10 µM
GLB	Glabridin	1,49	10 µM
GRA	beta Glycyrrhetinic acid	0,94	10 µM
IAA	Isoangustone A	1,07	10 µM
GLYC	Glyasperin C	1,06	10 µM
XN	Xanthohumol	0,90	10 µM
IXN	Isoxanthohumol	0,83	10 µM
IXNO	Isoxanthohumol oxime	0,92	10 µM
AMF1	Amorfrutin 1	0,83	10 µM
AMF2	Amorfrutin 2	0,83	10 µM
CBD	Cannabidiol	0,86	10 µM
HU331	HU331	0,00	10 µM
CBN	Cannabinol	0,46	10 µM
CBGA	Cannabigerolic acid	0,89	10 µM
CBDA	Cannabidiolic acid	0,83	10 µM
CBNA	Cannabinolic acid	1,03	10 µM
CANB	Cannflavin B	0,86	10 µM
Pinoresinol		1,01	10 µM
Neoabietic acid		1,05	10 µM
GalapaHM_D_1		1,53	10 µM
GalapaHM_EaBu_1		1,27	10 µM
GalodoHM_D_1		1,38	10 µM
GalodoHM_EaBu_1		1,12	10 µM
GalsylHM_D_1		1,40	10 µM
GalsylHM_EaBu_1		1,17	10 µM
GalalbHM_D_1		1,28	10 µM
GalalbHM_EaBu_1		1,12	10 µM
STK743870		0,63	10 µM

Abbreviation List

Abbreviation	Full term
AF	Activation function
ATRA	All-trans retinoic acid
ATP	Adenosine-5'-triphosphate
BMAL1	Brain and muscle ARNT-like 1
CLOCK	Circadian locomotor output cycles protein kaput

Abbreviation	Full term
CoA	Coenzyme A
CRY	Cryptochrome
DBD	DNA-binding domain
DMEM	Dulbecco's Modified Eagle's Medium
DMSO	Dimethyl sulfoxide
DNTI	Drugs from Nature Targeting Inflammation
DOR	Dimeric orphan receptor
DTT	Dithiothreitol
EC_{50}	Half-maximal effective concentration
EDTA	Ethylenediaminetetraacetic acid
eGFP	Enhanced green fluorescent protein
E_{max}	Maximal effect
FA	Fold activation
FBS	Fetal bovine serum
FGF21	Fibroblast growth factor 21
Gal4	Galactose-responsive transcription factor 4
GCNF	Germ cell nuclear factor
HBS	HEPES-buffered saline
HDL	High-density lipoprotein
HEK293	Human embryonic kidney 293 cells
HSP	Heat-shock protein
IC_{50}	Half-maximal inhibitory concentration
IL	Interleukin
I_{max}	Maximal Inhibition
LBD	Ligand-binding domain
LXR	Liver X receptor
MOR	Monomeric orphan receptor
PBS	Phosphate-buffered saline
PER	Period circadian clock gene
PPAR	Peroxisome proliferator-activated receptor
RAR	Retinoic acid receptor
REV-ERB	Reverse-Erb receptor
RFU	Relative fluorescence units
ROR	Retinoic acid receptor-related orphan receptor
RORα	Retinoic acid receptor-related orphan receptor alpha
RORβ	Retinoic acid receptor-related orphan receptor beta
RORγ	Retinoic acid receptor-related orphan receptor gamma
RORγt	Retinoic acid receptor-related orphan receptor gamma t

Abbreviation	Full term
RORE	ROR response element
Runx2	Runt-related transcription factor 2
RXR	Retinoid X receptor
SD	Standard deviation
STAT3	Signal transducer and activator of transcription 3
TGF-β	Transforming growth factor beta
TH17	T helper 17 cell
UAS	Upstream activating sequence
VDR	Vitamin D receptor

List of Figures

List of Tables

9 Acknowledgements

I would like to sincerely thank my supervisor Univ.-Prof. Verena Dirsch for giving me the opportunity to complete my master's thesis in the Department of Pharmaceutical Sciences, Division of Pharmacognosy, and within her research group. I am grateful for the chance to gain insight into scientific work and to contribute to a project in the field of molecular pharmacology and natural products research.

I am especially thankful to Mag. Dr. Patrik Schwarz for his supervision, scientific guidance, and constructive feedback throughout this thesis. His support helped me to better understand the experimental approaches and to improve the interpretation and presentation of my results. I would also like to thank MSc. Lorenza Bertaina for her constant support during my practical work in the laboratory. I greatly appreciated her patience, helpful explanations, and encouragement throughout the experimental part of this thesis. I am very thankful to both of them for the friendly and humorous working atmosphere, which made even long days in the laboratory pass quickly.

Many thanks also go to the entire Molecular Targets group for their help, kindness, and welcoming atmosphere. I am very grateful for the support I received in the laboratory and for the positive working environment.

Finally, I would like to thank my family and friends for their encouragement, understanding, and support throughout my studies.

10 Danksagung

Zunächst möchte ich mich herzlich bei meiner Betreuerin Univ.-Prof. Verena Dirsch bedanken, die mir die Möglichkeit gegeben hat, meine Masterarbeit am Department für Pharmazeutische Wissenschaften, Abteilung Pharmakognosie, und in ihrer Forschungsgruppe durchzuführen. Ich bin sehr dankbar für die Gelegenheit, Einblicke in die wissenschaftliche Forschung zu gewinnen und an einem Projekt im Bereich der molekularen Pharmakologie und Naturstoffforschung mitzuarbeiten.

Ein besonderer Dank gilt Mag. Dr. Patrik Schwarz für seine Betreuung, wissenschaftliche Unterstützung und das konstruktive Feedback während der gesamten Masterarbeit.

Seine Anregungen haben wesentlich dazu beigetragen, die experimentellen Ansätze besser zu verstehen sowie die Ergebnisse kritisch zu interpretieren und aufzubereiten. Ebenso möchte ich MSc. Lorenza Bertaina herzlich für ihre kontinuierliche Unterstützung im Labor danken. Ich habe ihre Geduld, ihre hilfreichen Erklärungen und ihre motivierende Art während des praktischen Teils dieser Arbeit sehr geschätzt. Auch möchte ich mich bei beiden für die freundliche und humorvolle Arbeitsatmosphäre bedanken, durch die selbst lange Tage im Labor wie im Flug vergangen sind.

Ein herzliches Dankeschön gilt außerdem der gesamten Molecular Targets Group für die Hilfsbereitschaft, die angenehme Arbeitsatmosphäre und die freundliche Aufnahme im Team. Die Unterstützung und das positive Umfeld haben meine Zeit im Labor zu einer sehr schönen Erfahrung gemacht.

Abschließend möchte ich meiner Familie und meinen Freunden für ihre Unterstützung, ihr Verständnis und ihren Zuspruch während meines Studiums und während der Erstellung dieser Masterarbeit danken.

11 References

1. Ottow E, Weinmann H. Nuclear receptors as drug targets. Weinheim: Wiley-VCH Verlag; 2008. (Methods and principles in medicinal chemistry; no. 39). doi:10.1002/9783527623297

2. Weikum ER, Liu X, Ortlund EA. The nuclear receptor superfamily: A structural perspective. Protein Sci. 2018;27(11):1876–92. doi:10.1002/pro.3496

3. Porter BA, Ortiz MA, Bratslavsky G, Kotula L. Structure and Function of the Nuclear Receptor Superfamily and Current Targeted Therapies of Prostate Cancer. Cancers. 2019 Dec;11(12):1852. doi:10.3390/cancers11121852

4. Zhang Y, Luo X yu, Wu D hai, Xu Y. ROR nuclear receptors: structures, related diseases, and drug discovery. Acta Pharmacol Sin. 2015 Jan;36(1):71–87. doi:10.1038/aps.2014.120

5. Burris TP, Busby SA, Griffin PR. Targeting Orphan Nuclear Receptors for Treatment of Metabolic Diseases and Autoimmunity. Chem Biol. 2012 Jan 27;19(1):51–9. doi:10.1016/j.chembiol.2011.12.011

6. Jetten AM. Retinoid-related orphan receptors (RORs): critical roles in development, immunity, circadian rhythm, and cellular metabolism. Nucl Recept Signal. 2009;7:e003. doi:10.1621/nrs.07003

7. Liu H, Aramaki M, Fu Y, Forrest D. Retinoid-Related Orphan Receptor β and Transcriptional Control of Neuronal Differentiation. In: Current Topics in Developmental Biology [Internet]. Elsevier; 2017 [cited 2026 May 4]. p. 227–55. Available from: https://linkinghub.elsevier.com/retrieve/pii/S0070215316301958 doi:10.1016/bs.ctdb.2016.11.009

8. Roforth MM, Khosla S, Monroe DG. Identification of Rorβ targets in cultured osteoblasts and in human bone. Biochem Biophys Res Commun. 2013 Nov 1;440(4):10.1016/j.bbrc.2013.10.006. doi:10.1016/j.bbrc.2013.10.006 PubMed Central PMCID: PMC3856899.

9. Schierle S, Merk D. Development of Nuclear Receptor Modulators. Methods Mol Biol. 2018;1824:245–60. doi:10.1007/978-1-4939-8630-9_14

10. Mangelsdorf DJ, Thummel C, Beato M, Herrlich P, Schütz G, Umesono K, et al. The nuclear receptor superfamily: The second decade. Cell. 1995 Dec;83(6):835–9. doi:10.1016/0092-8674(95)90199-X

11. Huang P, Chandra V, Rastinejad F. Structural Overview of the Nuclear Receptor Superfamily: Insights into Physiology and Therapeutics. Annu Rev Physiol. 2010 Mar 17;72(1):247–72. doi:10.1146/annurev-physiol-021909-135917

12. A Unified Nomenclature System for the Nuclear Receptor Superfamily. Cell. 1999 Apr;97(2):161–3. doi:10.1016/S0092-8674(00)80726-6

13. Cyr P, Bronner SM, Crawford JJ. Recent progress on nuclear receptor RORγ modulators. Bioorg Med Chem Lett. 2016 Sep 15;26(18):4387–93. doi:10.1016/j.bmcl.2016.08.012

14. Becker-André M, André E, DeLamarter JF. Identification of nuclear receptor mRNAs by RT-PCR amplification of conserved zinc-finger motif sequences. Biochem Biophys Res Commun. 1993 Aug 16;194(3):1371–9. doi:10.1006/bbrc.1993.1976

15. Ladurner A, Schwarz PF, Dirsch VM. Natural products as modulators of retinoic acid receptor-related orphan receptors (RORs). Nat Prod Rep. 2021;38(4):757–81. doi:10.1039/D0NP00047G

16. Ivanov II, McKenzie BS, Zhou L, Tadokoro CE, Lepelley A, Lafaille JJ, et al. The Orphan Nuclear Receptor RORγt Directs the Differentiation Program of Proinflammatory IL-17+ T Helper Cells. Cell. 2006 Sep 22;126(6):1121–33. doi:10.1016/j.cell.2006.07.035

17. Solt LA, Burris TP. Action of RORs and Their Ligands in (Patho)physiology. Trends Endocrinol Metab TEM. 2012 Dec;23(12):619–27. doi:10.1016/j.tem.2012.05.012

18. Kojetin DJ, Burris TP. REV-ERB and ROR nuclear receptors as drug targets. Nat Rev Drug Discov. 2014 Mar;13(3):197–216. doi:10.1038/nrd4100

19. Huang M, Bolin S, Miller H, Ng HL. RORγ Structural Plasticity and Druggability. Int J Mol Sci. 2020 Jul 27;21(15):5329. doi:10.3390/ijms21155329

20. Stehlin-Gaon C, Willmann D, Zeyer D, Sanglier S, Van Dorsselaer A, Renaud JP, et al. All-trans retinoic acid is a ligand for the orphan nuclear receptor RORβ. Nat Struct Mol Biol. 2003 Oct;10(10):820–5. doi:10.1038/nsb979

21. Stehlin C, Wurtz J, Steinmetz A, Greiner E, Schüle R, Moras D, et al. X-ray structure of the orphan nuclear receptor RORβ ligand-binding domain in the active conformation. EMBO J. 2001 Nov 1;20(21):5822–31. doi:10.1093/emboj/20.21.5822

22. Santori FR, Huang P, van de Pavert SA, Douglass EF, Leaver DJ, Haubrich BA, et al. Identification of natural RORγ ligands that regulate the development of lymphoid cells. Cell Metab. 2015 Feb 3;21(2):286–98. doi:10.1016/j.cmet.2015.01.004

23. Schultz JR, Tu H, Luk A, Repa JJ, Medina JC, Li L, et al. Role of LXRs in control of lipogenesis. Genes Dev. 2000 Nov 15;14(22):2831–8. doi:10.1101/gad.850400

24. Kumar N, Solt LA, Conkright JJ, Wang Y, Istrate MA, Busby SA, et al. The Benzenesulfoamide T0901317 [N-(2,2,2-Trifluoroethyl)-N-[4-[2,2,2-trifluoro-1-hydroxy-1-(trifluoromethyl)ethyl]phenyl]-benzenesulfonamide] Is a Novel Retinoic Acid Receptor-Related Orphan Receptor-α/γ Inverse Agonist. Mol Pharmacol. 2010 Feb;77(2):228–36. doi:10.1124/mol.109.060905

25. Wang Y, Kumar N, Nuhant P, Cameron MD, Istrate MA, Roush WR, et al. Identification of SR1078, a Synthetic Agonist for the Orphan Nuclear Receptors RORα and RORγ. ACS Chem Biol. 2010 Nov 19;5(11):1029–34. doi:10.1021/cb100223d

26. Solt LA, Kumar N, Nuhant P, Wang Y, Lauer JL, Liu J, et al. Suppression of TH17 differentiation and autoimmunity by a synthetic ROR ligand. Nature. 2011 Apr;472(7344):491–4. doi:10.1038/nature10075

27. Kumar N, Lyda B, Chang MR, Lauer JL, Solt LA, Burris TP, et al. Identification of SR2211: A Potent Synthetic RORγ-Selective Modulator. ACS Chem Biol. 2012 Apr 20;7(4):672–7. doi:10.1021/cb200496y

28. Doebelin C, Patouret R, Garcia-Ordonez RD, Chang MR, Dharmarajan V, Novick S, et al. Identification of potent RORβ modulators: Scaffold variation. Bioorg Med Chem Lett. 2018 Oct;28(19):3210–5. doi:10.1016/j.bmcl.2018.08.017

29. Schwarz PF, Perhal AF, Schöberl LN, Kraus MM, Kirchmair J, Dirsch VM. Identification of the Natural Steroid Sapogenin Diosgenin as a Direct Dual-Specific RORα/γ Inverse Agonist. Biomedicines. 2022 Aug 25;10(9):2076. doi:10.3390/biomedicines10092076

30. Chang MR, Griffin PR. RORβ modulates a gene program that is protective against articular cartilage damage. Tomaszewska E, editor. PLOS ONE. 2022 Oct 13;17(10):e0268663. doi:10.1371/journal.pone.0268663

31. Dong C. TH17 cells in development: an updated view of their molecular identity and genetic programming. Nat Rev Immunol. 2008 May;8(5):337–48. doi:10.1038/nri2295

32. Jetten AM, Cook DN. (Inverse) Agonists of Retinoic Acid–Related Orphan Receptor γ: Regulation of Immune Responses, Inflammation, and Autoimmune Disease. Annu Rev Pharmacol Toxicol. 2020 Jan 6;60:371–90. doi:10.1146/annurev-pharmtox-010919-023711

33. Jin W, Dong C. IL-17 cytokines in immunity and inflammation. Emerg Microbes Infect. 2013 Sep;2(9):e60. doi:10.1038/emi.2013.58

34. Jetten AM, Kang HS, Takeda Y. Retinoic acid-related orphan receptors α and γ: key regulators of lipid/glucose metabolism, inflammation, and insulin sensitivity. Front Endocrinol. 2013 Jan 25;4:1. doi:10.3389/fendo.2013.00001

35. Kim K, Boo K, Yu YS, Oh SK, Kim H, Jeon Y, et al. RORα controls hepatic lipid homeostasis via negative regulation of PPARγ transcriptional network. Nat Commun. 2017 Jul 31;8(1):162. doi:10.1038/s41467-017-00215-1

36. Meissburger B, Ukropec J, Roeder E, Beaton N, Geiger M, Teupser D, et al. Adipogenesis and insulin sensitivity in obesity are regulated by retinoid-related orphan receptor gamma. EMBO Mol Med. 2011 Nov;3(11):637–51. doi:10.1002/emmm.201100172

37. André E, Gawlas K, Becker-André M. A novel isoform of the orphan nuclear receptor RORbeta is specifically expressed in pineal gland and retina. Gene. 1998 Aug 31;216(2):277–83. doi:10.1016/s0378-1119(98)00348-5

38. André E, Conquet F, Steinmayr M, Stratton SC, Porciatti V, Becker-André M. Disruption of retinoid-related orphan receptor β changes circadian behavior, causes retinal degeneration and leads to vacillans phenotype in mice. EMBO J. 1998 Jul 15;17(14):3867–77. doi:10.1093/emboj/17.14.3867

39. Waltenberger B, Atanasov AG, Heiss EH, Bernhard D, Rollinger JM, Breuss JM, et al. Drugs from nature targeting inflammation (DNTI): a successful Austrian interdisciplinary network project. Monatshefte Chem. 2016;147:479–91. doi:10.1007/s00706-015-1653-y

40. Fan F, Wood KV. Bioluminescent assays for high-throughput screening. Assay Drug Dev Technol. 2007 Feb;5(1):127–36. doi:10.1089/adt.2006.053

41. Schmitz S, Desel C. Der Experimentator Zellbiologie [Internet]. Berlin, Heidelberg: Springer; 2018 [cited 2026 Apr 7]. Available from: http://link.springer.com/10.1007/978-3-662-56111-9 doi:10.1007/978-3-662-56111-9

42. Paguio A, Stecha P, Wood KV, Fan F. Improved dual-luciferase reporter assays for nuclear receptors. Curr Chem Genomics. 2010;4:43–9. doi:10.2174/1875397301004010043

43. Luckert C, Hessel S, Lampen A, Braeuning A. Utility of an appropriate reporter assay: Heliotrine interferes with GAL4/upstream activation sequence-driven reporter gene systems. Anal Biochem. 2015 Oct 15;487:45–8. doi:10.1016/j.ab.2015.07.009

44. Kwon M, Firestein BL. DNA transfection: calcium phosphate method. Methods Mol Biol. 2013;1018:107–10. doi:10.1007/978-1-62703-444-9_10

45. Thangaraju P, Varthya SB. ISO 10993: Biological Evaluation of Medical Devices. In: Timiri Shanmugam PS, Thangaraju P, Palani N, Sampath T, editors. Medical Device Guidelines and Regulations Handbook [Internet]. Cham: Springer International Publishing; 2022 [cited 2026 Jun 10]. p. 163–87. Available from: https://link.springer.com/10.1007/978-3-030-91855-2_11 doi:10.1007/978-3-030-91855-2_11

46. Riss T, Niles A, Minor L. Cell Viability Assays Assay Guidance Manual. Assay Guid Man. 2004 Jan 1;1–23.

47. O'Brien J, Wilson I, Orton T, Pognan F. Investigation of the Alamar Blue (resazurin) fluorescent dye for the assessment of mammalian cell cytotoxicity. Eur J Biochem. 2000;267(17):5421–6. doi:10.1046/j.1432-1327.2000.01606.x

48. Uzarski JS, DiVito MD, Wertheim JA, Miller WM. Essential design considerations for the resazurin reduction assay to noninvasively quantify cell expansion within perfused extracellular matrix scaffolds. Biomaterials. 2017 Jun;129:163–75. doi:10.1016/j.biomaterials.2017.02.015

49. Pastwińska J, Karaś K, Sałkowska A, Karwaciak I, Chałaśkiewicz K, Wojtczak BA, et al. Identification of Corosolic and Oleanolic Acids as Molecules Antagonizing the

Human RORγT Nuclear Receptor Using the Calculated Fingerprints of the Molecular Similarity. Int J Mol Sci. 2022 Feb 8;23(3):1906. doi:10.3390/ijms23031906